Report Date: Oct 10, 2004

Semi-Annual Technical Progress Report

INVESTIGATION OF EFFICIENCY IMPROVEMENTS DURING CO_2 INJECTION IN HYDRAULICALLY AND NATURALLY FRACTURED RESERVOIRS

DOE Contract No.: DE-FC26-01BC15361

Harold Vance Department of Petroleum Engineering
Texas A& M University
3116 TAMU
College Station, TX 77843-3116
(979) 845-2241

Contract Date:	September 28, 2001
Anticipated Completion Date:	September 27, 2005
Principal Investigator:	David S. Schechter Harold Vance Department of Petroleum Engineering
Contracting Officer's Representative:	Dan Ferguson National Petroleum Technology Office
Report Period:	April 1, 2004-Sept 30, 2004

DISCLAIMER

ABSTRACT

This report describes the work performed during the third year of the project, "Investigating of Efficiency Improvements during CO_2 Injection in Hydraulically and Naturally Fractured Reservoirs." The objective of this project is to perform unique laboratory experiments with artificial fractured cores (AFCs) and X-ray CT to examine the physical mechanisms of bypassing in HFR and NFR that eventually result in more efficient CO_2 flooding in heterogeneous or fracture-dominated reservoirs. To achieve this objective, in this period we concentrated our effort on modeling fluid flow through rough fractures and investigating the grid orientation effect in rectangular grid blocks particularly at high mobility ratio as our precursor to use a compositional simulator. We are developing a robust simulator using Voronoi grids to accurately represent natural and induced fractures. We are also verifying the accuracy of the simulation using scaled laboratory experiments to provide a benchmark for our simulation technique. No such simulator currently exists so this capability will represent a major breakthrough in simulation of gas injection in fractured systems. The following sections outline the results that appear in this report.

Simulation of Fluid Flow through Rough Fractures

Flow through a fracture is usually assumed to take place between two smooth parallel plates. However, it is widely accepted that the fracture has tortuous paths as a result of surface roughness and hence the flow behavior in these paths compared to that in parallel plates is different. Although previous studies have shown that the fracture aperture follows lognormal distribution, studies have not been conducted to determine the distribution of fracture aperture with changes in stress conditions. In this paper, we present fracture aperture measurements under different stress conditions using an X-Ray CT scanner. We developed a calibration curve to obtain a correlation between CT numbers and fracture aperture since there is no direct calculation of aperture from CT scanner data. Aperture distribution patterns from about six thousand aperture measurements were obtained for each stress condition evaluated. The results of this study show that the apertures follow lognormal distribution even at elevated stress conditions. We then performed waterflood experiments as a precursor to CO_2 injection to validate the use of distributed apertures in simulators. A sensitivity analysis was also performed to analyze the effect of injection rates and fracture roughness on oil recovery.

A Unique Grid-Block System for Improved Grid Orientation

The grid orientation effect is a long-standing problem plaguing reservoir simulators that employ finite difference schemes. A rotation of the computational grids yields a substantially different solution under certain circumstances, such as adverse mobility ratio. For example, in a five-spot pattern, the predicted recovery, water cut performance and the locations of the fronts depend on the type of grid system used. A Cartesian grid with one axis parallel to the line joining an injector and producer gives a solution significantly different from a grid that has the axes oriented at 45° to this line.

The objective of this study is to develop a grid system that can improve the representation of the configuration, thus minimizing the grid orientation effect. This section presents a method for reducing the effect of grid orientation on computed

numerical results in finite difference reservoir simulation. This method involves using a unique grid-block assignment where rectangular grid blocks are interspersed with octagonal grid blocks. The boundaries are then populated with triangular grid blocks. Thus, the entire domain will consist of a “structured” grid block system referred to as the Hybrid Grid Block (HGB).

To test the viability of HGB, a finite difference IMPES-formulated two-dimensional black oil simulator was developed in this study, while retaining the familiar finite-difference discretization of the flow equations. Simulation cases were conducted to further examine the grid orientation effect in conventional grid block systems. Then, similar cases are run using HGB grid system. The outcome shows that HGB gives very close agreement between the parallel and diagonal grid orientation. This innovative grid block assignment will help to reduce the grid orientation effects compared to conventional grid block system.

TABLE OF CONTENTS

LIST OF TABLES

LIST OF FIGURES

ACKNOWLEDGMENTS

Financial support for this work is provided by the United States Department of Energy (NPTO/National Petroleum Technology Office). This support is gratefully acknowledged.

I greatly appreciate diligent efforts from the following individuals who contributed to this project: Erwinsyah Putra helped with the technical part of this research, Deepak Chakravarty and Vivek Muralidharan conducted experimental and simulation work on the X-Ray CT scanner as described in Chapter 1 and Emeline Chong and Zuher Syihab conducted numerical modeling as described in Chapter 2.

EXECUTIVE SUMMARY

This report describes the work performed during the third year of the project, "Investigating of Efficiency Improvements during CO_2 Injection in Hydraulically and Naturally Fractured Reservoirs." The objective of this project is to perform unique laboratory experiments with artificial fractured cores (AFCs) and X-ray CT to examine the physical mechanisms of bypassing in HFR and NFR that eventually result in more efficient CO_2 flooding in heterogeneous or fracture-dominated reservoirs.

This report provides results of the sixth semi-annual technical progress report that consists of (1) modeling laboratory experiments and (2) numerical modeling to investigate the grid orientation effect in Cartesian grid blocks that usually occurs when high mobility ratio case is used in reservoir simulation. Within the project objectives, the specific goals for this period are (1) to validate the use of distributed apertures in multiphase flow study and to analyze the effect of injection rates and fracture roughness on oil recovery, (2) to develop a grid system that can improve the representation of the fracture networks by minimizing the grid orientation effect.

In this report, we present the following work that has been performed to achieve the aforementioned goals. The first chapter is part of our paper that will appear at the 2004 SPE International Petroleum Conference in Mexico held in Puebla, Mexico, 8–9 November 2004. In this chapter, we investigated the displacement of oil by water using our X-ray CT scanner in fractured cores. We conducted the experiments at various injection rates and scanned the core being flooded at certain times. We recorded oil and water produced at the outlet point. We performed two simulation runs using parallel plate model and distributed fracture aperture model and compared the results to experimental data. Once we achieve satisfactory matches, we performed sensitivity studies to analyze the effect of injection rates on apertures distribution on oil recovery and water breakthrough time. Important conclusions can be drawn from the work include:

1. Simulation results indicate that the parallel plate model fails to duplicate laboratory experiment performance hence this model does not adequately represent a fractured model.
2. On the other hand, satisfactory matches between simulation and experimental data using distributed aperture model shows this model provides an accurate description of a fractured model.
3. The water breakthrough time increases as fracture aperture and injection rate increase.
4. As the injection rate increases the difference in the oil recoveries predicted by the two models magnifies.
5. At large aperture sizes, the performance of the parallel plate model becomes closer to that of the distributed aperture model. This indicates that there is a certain critical fracture aperture where both models would give similar results.

The second chapter is part of our paper that will appear at the SPE Asia Pacific Oil and Gas Conference and Exhibition held in Perth, Australia, 18–20 October 2004. In this chapter, we developed a finite difference IMPES-formulated two dimensional black oil

simulator using both Cartesian grid block system and a unique grid block system called Hybrid Grid Model (HGB). We compared the viability of this simulator using Cartesian grid block system with a commercial simulator Eclipse™. We examined the grid orientation in conventional grid block system and then we ran simulation cases using the HGB grid system. Important conclusions can be drawn from the work include:

1. The grid orientation effect was observed in rectangular Cartesian grid models even with isotropic and homogeneous reservoirs with favorable mobility ratio.
2. Grid refinement can help to minimize the grid orientation effect in rectangular Cartesian grid models when there are favorable mobiliy ratios, ie. M=1.0 or less. However, at an unfavorable mobility ratio, neither the parallel, diagonal grid orientation, nor grid refinement is effective in reducing the grid orientation effect.
3. HGB grid is able to minimize the grid orientation effect even for unfavorable mobility ratio displacement problems, with relative difference of about 6% for all the cases run.

Project Fact Sheet

Progress work efforts at Project Fact Sheet are listed in Appendix A.

Chapter I

Simulation of Fluid Flow through Rough Fractures

1.1 Introduction

Modeling of fluid flow through rough fractures has gained importance over the years. This can be attributed to the extremely low ultimate recoveries obtained from naturally fractured reservoirs, in spite of their huge reserves. Attempts are being made to develop efficient models to better formulate depletion plans. The first comprehensive work on flow through open fractures was done by Lomize[1], in which he used parallel glass plates and demonstrated the validity of cubic law for laminar flow. He modeled fluid flow with different fracture shapes and investigated the effects of changing the fracture walls from smooth to rough.

Witherspoon *et al.*[2] conducted laboratory experiments to validate parallel plate theory and they showed that the parallel plate approximation tends to break down at higher normal stress (>10 MPa) across the fracture. Alfred[3] also confirmed that the parallel plate assumption is not valid to adequately model the fluid flow experiments when overburden pressure is significant. The flow through a single fracture does not progress uniformly as assumed by parallel plate theory; rather, it flows through a limited number of channels[4,5]. Hence, the fluid flow in these tortuous channels tends to follow a preferred path. Pyrak *et al.*[6] (1985) performed laboratory experiments wherein they injected molten wood's metal into single fractures at different applied stress conditions. The direct evidence of tortuous paths was observed upon opening the cooled metal in the fracture. The fluid flow in these paths will be through the larger apertures which offer least resistance to flow.

When the parallel plate approach was proved invalid, Tsang and Witherspoon[5] accounted for the variation of apertures in a rough fracture. Later, Tsang[4] modeled the variation of fracture apertures by electrical resistors with different resistance values placed on a two-dimensional grid. The results indicated that smaller apertures play a key role in restricting fluid flow. When the fracture contact area increases, tortuosity and connectivity of fractures become important. The flow through a single fracture took place in a limited number of channels, which was evident from the field experiment carried out in a single

fracture[7]. Gentier[8] measured fracture surface roughness profiles in a granite fracture. Upon plotting the apertures, the aperture density distribution was approximated by a gamma function. The density distribution is given by

$$n(b) = \frac{1}{b_o^2} b \exp(-b/b_o) \quad \text{.....(1.1)}$$

where b_o represents the distribution peaks, and the mean aperture is $2b_o$. The same distribution was assumed when considering the channeling of flow through fractured media[9]. Tsang and Tsang[9] assumed the channel width to be a constant of the same order as the correlation length λ, where correlation length is the spatial length within which the apertures have similar values. The reduction in channel apertures affected the tracer breakthrough curves when normal stress across a fracture was increased.

Although gamma distribution was considered, some authors[7,10] observed a lognormal distribution of fracture apertures from well logs and experiments conducted on cores. Later Moreno *et al.*[11] followed the lognormal approach when conducting flow and tracer transport model in a single fracture. Using the approach, the flow patterns showed strong resemblance to field observations reported by Bourke[12]. Tsang and Tsang[13] used lognormal approach to distribute fracture apertures for obtaining a relationship between flow and transport measurements of variable apertures. The frequency of the lognormal distribution is written as follows[14]:

$$f(x) = \frac{1}{x\sqrt{2\pi\beta^2}} \exp\left[\frac{-(\ln x - \alpha)^2}{2\beta^2}\right] \quad \text{.....(1.2)}$$

where,

$$\beta^2 = \ln\left(1 + \frac{\sigma^2}{\delta^2}\right) \quad \text{.....(1.3)}$$

and

$$\alpha = \ln\delta - \frac{\beta^2}{2} \quad \text{.....(1.4)}$$

The mean aperture was determined from fluid flow measurements and this value was used to distribute the apertures lognormally. The aperture variance was determined from tracer breakthrough. Alfred *et al.*[14] also assumed lognormal distribution for fracture

apertures to account for fracture roughness. Keller[15] imaged fracture apertures using an X-ray CT scanner. Based on the study using three different cores, he concluded that the fractures follow a lognormal distribution.

Fracture properties are strongly affected by changes in stress conditions and therefore the effect of stress acting on the reservoirs should be considered in obtaining fracture aperture distributions. Even though extensive research has been done on fracture aperture distributions, the effect of varying stress conditions has not yet been investigated. Stress changes aperture size and might have an effect on the distribution of fracture apertures. Thus, the aim of this study is to measure fracture apertures under different stress conditions using an X-ray CT scanner. Several feeler gauges were used to create fractures of known size and obtain a calibration curve. Once the calibration curve was obtained, fracture aperture distributions from a fractured core were measured under different overburden pressures. Probability distributions of fracture apertures were examined to obtain the mean aperture and variance values. Using those values, the probability distributions of density function were plotted to determine the distribution of fracture apertures at each overburden pressure.

Waterflooding was then performed using a fractured core to validate the use of lognormal approach for fracture apertures and to prove that the parallel plate model is not valid for modeling fluid flow through rough surface.

1.2 Calibration Technique

A Picker 4th generation CT scanner was used for imaging the core samples. The power, voltage and algorithm requirements were chosen typical of a sandstone sample. An X-ray CT scanner identifies density differences between various objects[16]. As the density of a fluid is less compared to the density of rock, the X-ray scans can be used to clearly distinguish a fluid filled fracture from the matrix. Although a clear visualization of fracture and matrix is possible, the CT numbers (dimensionless numbers that are functions of densities) do not represent any physical characteristic. In order to obtain the fracture aperture measurement, a calibration technique has to be used to correlate the CT numbers with the actual aperture size. Keller[17] made use of non-intrusive imaging to obtain aperture

calibration curves for granite and sandstone. Using the curve, fracture apertures as small as 35μm could be measured. A similar technique was followed by He[18] in 1998. Both techniques use the integrated CT signal to determine fracture aperture. The integration was done by summing up the differences between a minimum rock CT number and the CT numbers pertaining to the fracture. Our calibration curve was developed based on this existing technique.

The experimental setup consists of two halves of the rock sample (Berea Core), feeler gauges and core holding equipment. The two halves were polished thoroughly to reduce surface roughness as much as possible. Smooth surfaces ensure that there is a proper match between the halves and hence smaller fractures can be measured. Feeler gauges were then placed between the two flat surfaces to create different fracture widths (Fig. 1.1). The following sizes of feeler gauges were used in the calibration experiment: 38 μm, 51 μm, 64 μm, 76 μm, 102 μm, 127 μm, 152 μm, 178 μm, 508 μm, and 813 μm.

The core sample with fracture was inserted into a sleeve to avoid artefact effects and held in the core holder. Multiple scans were then taken along the length of the core, perpendicular to the longitudinal axis. Fig. 1.2A shows a typical set of scans for the Berea sample with 38 mm fracture size. The color variations indicate variable densities in the sample, with the relatively high density steel feeler gauge set to bright pink color, the less dense rock material set to a bright orange color and the lower densities set to green, blue and black in decreasing order of densities. First scan in Fig. 1.2A is taken through the steel feeler gauge placed on one end of core sample; hence the color appears brighter in the middle of the core. Both ends of core sample have a feeler gauge and scans were taken starting from one feeler gauge to the start of the next feeler gauge, with intervals of 5 mm. The next three scans show a fracture aperture of 38 μm along the length of the core. The dip in CT number curve in the middle corresponds to the location of the fracture region and this clearly distinguishes fracture from the matrix. Since this dip (Fig. 1.3) corresponds to a fracture size of 38 μm, a correlation can be obtained between the area enclosed by the curve and the fracture size. The dip is not abrupt, but rather a smooth transition from matrix to fracture. This effect is due to dispersion of CT numbers, which is caused due to a finite beam width and oversampling. Fig. 1.2B shows the fracture aperture size of 102 μm, along the length of the core. As the aperture size increases, the CT number decreases and

the fracture aperture can be seen clearly in the middle of the core, with a darker color. Fig. 1.4 shows a comparison of the average CT number curves obtained for various fracture sizes.

1.3 Calibration Curve

A plot of CT number versus the pixel number was made based on the CT numbers obtained from each scan. An average CT number plot was obtained to account for minor variations in fracture sizes caused by surface roughness. An example of such plot is shown in Fig. 1.5. From this plot, a threshold CT number was identified, which essentially is the minimum rock CT number. All the CT numbers in the area below the minimum rock CT number are subtracted from the rock CT number and the differences are used to obtain the integrated CT signal for the fracture size. The integrated CT signals are calculated for each pixel number and are given an index starting from 1 to n as shown in Fig. 1.5. The area of integrated CT region is calculated from the following formula:

For index i equal to 1 to c,

$$Area(i) = IntCT(i-1) + \frac{1}{2}[IntCT(i) - IntCT(i-1)] \quad \text{.....(1.5)}$$

For index i equal to c+1 to n,

$$Area(i) = IntCT(i) + \frac{1}{2}[IntCT(i-1) - IntCT(i)] \quad \text{.....(1.6)}$$

After measuring nine different feeler gauges, we obtained a calibration curve for fracture aperture (Fig. 1.6). The plot shows a linear relationship between the integrated CT signal and fracture aperture. The linear relationship holds even at small fracture apertures. The equation obtained from this calibration curve is,

$$y = 8.7616x + 460.7 \quad \text{.....(1.7)}$$

By rearranging the equation we can calculate fracture aperture, using the integrated CT signal as follows:

$$x = 0.1141y - 52.582 \quad \text{.....(1.8)}$$

Given a fracture sample, the fracture apertures can be measured using the calibration curve.

1.4 Fracture Aperture Distribution

For this specific experiment we used a 1 inch diameter by 2.36 inch length of Berea core. The core was fractured mechanically in the laboratory. The artificially fractured core was then imaged using the X-ray CT scanner. Images were taken at 1 mm intervals along the length of the core. The core was then subjected to overburden pressure of 500 psi and scans were taken at the same locations. This procedure was repeated for overburden pressures of 1000 psi and 1500 psi. Fig. 1.7 shows the images taken with and without overburden pressures. About 6000 data points were taken for each overburden condition. The resulting CT numbers from the images were then converted to the aperture values using the calibration curve as discussed in the previous section. Mean, variance, and standard deviation were obtained for each dataset. A comparative study was made for different overburden pressures. The results are plotted in Fig. 1.8.

The apertures are distributed in the range of 0 to 2000 microns as shown in Fig. 1.8. The tail of the aperture distribution is long and the aperture distribution is right skewed which suggests that the distribution might follow either gamma or lognormal distribution as given in the earlier studies[8,9,15]. The tail of the apertures controls the fluid flow as fluid will tend to flow through preferred channels of least resistance[14]. Since most apertures fall in the range of 100 to 500 microns, the permeability measurements will largely be controlled by small apertures. The presence of some large apertures in the range of 600 to 2000 microns may provide the main path for the fluid flow if they are interconnected. The calculation of flow rate based on these measured permeabilities will be different from the calculation using a single mean value of permeability as assumed by parallel plate approach.

Using the mean and variance of the aperture values obtained from the probability distribution plot for each overburden pressure, the distributions of probability density function can be obtained by applying Eq. 1.2. The distribution plots are presented in Fig. 1.9. Comparison of actual dataset to calculated distribution reveals that the distribution of pdf follows lognormal distribution at all stresses.

Without applying an overburden pressure, the probability density function that follows lognormal distribution has a mean aperture value of 370.53 microns and a variance of

44847 (Fig. 1.9). This lognormal distribution confirms the previous findings[4,11,13,14,15]. As the overburden pressure increases, the mean and variance of the apertures decrease suggesting that the permeability decreases due to increase in overburden pressures. The mean of the apertures decreases drastically from 370.53 microns to 197.997 microns when an initial overburden pressure of 500 psi is applied.

The fracture surfaces are rough and have many contact points along the fracture. The contact points tend to breakdown under overburden stress. The decrease in aperture sizes is not significant with further increase in overburden pressures. Since each reservoir experiences different overburden pressures, this research will be important to identify some of the uncertainties in predicting fluid flow through fractured reservoirs.

1.5 Waterflooding Experiment

A clean, dry core was artificially fractured in the laboratory using the Brazilian technique. Fracture apertures were then determined using the method suggested in the previous sections. The core was then saturated with refined oil and inserted into a Hassler-type core holder with a confining pressure of 500 psia. Water was then injected at a rate of 0.2 cm^3/min. The core properties are given in Table 1.1. CT scans were taken before, during and at the end of the injection process. The first set of scans in Fig. 1.10 represents the cross-sectional CT images of the oil saturated core. The CT numbers for the oil saturated core are found to be in the range of 1450. When water injection is started, the water invasion can be seen as an increase in the CT numbers, as identified by a change in color (Fig. 1.10). Water injection was continued till residual oil saturation was reached. CT numbers of the water saturated core are seen to be in the range of 1650 to 1700. Due to high permeability of the fracture, water is seen to preferentially flow along the fracture plane. Fig. 1.11 shows the 3D water saturations along the length of the core.

1.5.1 Parallel Plate Simulation Model

A numerical model utilizing a commercial simulator (CMG^{TM}) was used to analyze the fluid flow through fracture during waterflooding. The laboratory process in which water was injected through the fracture was duplicated in this modeling effort, using the parallel plate assumption. The mean fracture aperture and the mean fracture permeability obtained

from the CT scanner data were treated as constant value in all the grid blocks in the fracture plane. 34x10x15 grid blocks were used for the simulation model. A well placed in gridblock 1,5,8 served as the water injector while the producers were placed on the matrix and the fracture layers at the outlet end.

Fig. 1.12 shows the comparison of fluid movement through fracture surface using X-ray profile and the simulated profile using parallel plate model. As we can see from the figure, the water saturation profiles predicted by parallel plate model indicate higher saturations compared to the CT profile. This difference can be attributed to the single mean value of fracture permeability used in the fracture. In this case, the fracture surface is devoid of roughness and contact points, which allows the water to move freely without any resistance to flow. This also results in an earlier breakthrough compared to what was observed during the experiment. The oil recovery was also lower compared to the experimental value (Fig. 1.13). Most of the injected water flows through the fracture and hence the predicted watercut is also higher than the observed watercut (Fig. 1.14).

1.5.2 Distributed Aperture Simulation Model

The distributed aperture simulation model was constructed with the same number of grid blocks and sizes as used in the parallel plate model. Actual aperture data was obtained from X-ray CT scanner results. Fig. 1.15 shows the 3D distribution of apertures along the fracture plane. The mean aperture size is 198 microns. Darker colors in the distribution pattern indicate higher aperture values.

The fracture aperture values were then converted to their corresponding fracture permeability values using the relation between fracture aperture and permeability[19] and introduced into the fracture layer with 34 x 10 gridblocks.

In this case, the fluid flows through the path of least resistance offered by the interconnected large apertures. The smaller apertures have lesser volumetric rate and offer resistance to flow, which diverts some amount of fluid into the matrix blocks. Fig. 1.16 shows the comparison of fluid flow profile obtained from the CT scanner and that obtained from simulation using the distributed aperture model. As can be seen from the figure, the water saturation profiles predicted by the distributed aperture model are in good agreement

with the CT profiles. Figs. 1.17 and 1.18 show that a good match is obtained between the observed and simulated oil recovery and water breakthrough. Fig. 1.18 also shows an improvement in the water cut match compared to the previous case. Fig. 1.19 shows the match obtained between observed and predicted cumulative water production.

1.5.3 Sensitivity Analysis

A sensitivity analysis was performed to analyze the effect of injection rates and aperture distributions on oil recovery and water breakthrough. Three different injection rates (0.2, 0.5, and 0.8 cm^3/min) were used with different aperture sizes for both parallel plate and distributed aperture model. About 2 PV of water was injected in each case. The oil recoveries obtained for each case have been tabulated in Table 1.2 and 1.3. Fig. 1.20 shows the effect of different injection rates on oil recovery. The oil recovery obtained is seen to decrease with an increase in the injection rate. This is due to an increase in the viscous forces, which causes the fluid to flow preferentially through the fracture layer with high values of permeability resulting in early breakthrough and poor sweep. At low injection rates, dominance of capillary forces over viscous forces results in delayed breakthrough and hence better recovery.

Changes in aperture distributions are also seen to affect oil recovery. The mean and variance values shown in Fig. 1.9 were used. For each distributed model case, the corresponding parallel plate model was constructed with the same value of mean and zero variance. It can be seen from Fig. 1.20 that, as the fracture aperture increases, the performance of the parallel plate model becomes closer to the distributed aperture model. The reason for this is the decrease in resistance to flow that was previously offered by the smaller apertures. Although the two models are in closer resemblance at lower injection rates, it is to be observed that the parallel plate model underestimates the oil recovery that can be obtained from the system. This shows that the oil recovery is very sensitive to the variance of aperture sizes, making the parallel plate model invalid for performance predictions.

1.6 Conclusions

The main conclusions derived from this study can be summarized as follows:

1. Fracture apertures follow lognormal distribution at all stress conditions.
2. Simulation results indicate that the parallel plate model does not adequately represent a fractured reservoir system.
3. The profile match obtained using the distributed aperture model shows that this model can be used to provide accurate descriptions of fractured systems.
4. Analysis of sensitivity to injection rates shows that, as the injection rate increases, the difference in the oil recoveries predicted by the two models also increases.
5. At higher injection rates, higher viscous forces cause early breakthrough from the fracture and hence the oil recovery obtained is lesser.
6. For large aperture sizes, the performance of the parallel plate model becomes closer to that of the distributed aperture model. The sensitivity of oil recovery to variance of aperture sizes makes the parallel plate model invalid.

Nomenclature

$Area(i)$ = Area of section i

b_o = Distribution peak

b = Aperture size

c = Index of lower CT number

$f(x)$ = Frequency of apertures

i = Index

$IntCT(i)$ = Integrated CT area for section i

n = Index of higher CT number

$n(b)$ = Probability density distribution

x = Fracture aperture

y = Total integrated CT signal

References

1. Lomize, G. M.: "Seepage in Fissured Rocks," State Press, Moskow-Leningrad, 1951.

2. Witherspoon, P. A., Wang, J. S. Y., Iwai, K., and Gale, J. E.: "Validity of Cubic Law for Fluid Flow in a Deformable Rock Fracture," *Water Resources Research*, 16(6), 1016-1024, 1980.
3. Alfred, D.: "Modeling Fluid Flow through a Single Fracture Using Experimental, Stochastic and Simulation Approaches," master's thesis, Texas A&M University, 2003.
4. Tsang, Y. W.: "The Effect of Tortuosity on Fluid Flow through a Single Fracture," *Water Resources Research*, 20(9), 1209-1215, 1984.
5. Tsang, Y. W. and Witherspoon, P. A.: "The Dependence of Fracture Mechanical and Fluid Properties on Fracture Roughness and Sample Size," *J. Geophysics. Res.*, 88(B3), 2359-2366, 1983.
6. Pyrak, L. R., Myer, L. R., and Cook, N. G. W.: "Determination of Fracture Void Geometry and Contact Area at Different Effective Stress," *Eos Trans.* AGU (abstract), 66(46), 903, 1985.
7. Bourke, P. J., Dunance, E. M., Heath, M. J., and Hodgkinson, D. D.: "Fracture Hydrology Relevant to Radionuclide Transport, AERE *Rep.* 11414, Atomic Energy Res. Estab., Harwell, United Kingdom, 1985.
8. Gentier, S.: "Morphologie et comportement hydromécanique d'une fracture naturelle dans un granite sous contrainte normale," doctoral thesis, Univ. d'Orléans, France, 1986.
9. Tsang, Y. W. and Tsang, C. F.: "Channel Model of Flow Through Fractured Media," *Water Resources Research*, 23(3), 467-479, 1987.
10. Bianchi, L. and Snow, D.: "Permeability Crystalline Rock Interpreted from Measured Orientations and Apertures of Fractures*," Annu. Arid Zone*, 8(2), 231-245, 1968.
11. Moreno, L., Tsang, Y. W., Tsang, C. F., Hale, F. V., and Neretnieks, I.: "Flow and Tracer Transport in a Single Fracture: A Stochastic Model and Its Relation to Some Field Observations," *Water Resources Research*, 24(12), 2033-2048, 1988.
12. Bourke, P. J.: "Channeling of Flow Through Fractures in Rock," in *Proceedings* of GEOVAL-87 International Symposium, Swed. Nucl. Power Inspectorate, Stockholm, Sweden, 1987.
13. Tsang, Y. W. and Tsang, C. F.: "Hydrological Characterization of Variable-Aperture Fractures," *Rock Joints*, Barton & Stephansson (eds), Balkema, Rotterdam, 1990.

14. Alfred, D., Putra, E., and Schechter, D.S.: "Modeling Fluid Flow through Single Fractures Using Experimental, Stochastic and Simulation Approaches," paper SPE/DOE 89442 presented at 2004 Improved Oil Recovery Symposium, OK, Tulsa, 17–21April.
15. Keller, A. A.: "Single and multiphase flow and transport in fractured porous media," PhD dissertation submitted to Stanford University (1996).
16. Wellington, S. L. and Vinegar, H. J.: "CT Studies of Surfactant- Induced CO_2 Mobility Control," paper SPE 14393 presented at the 1985 SPE Annual Technical Conference and Exhibition, Las Vegas, September 22-25.
17. Keller, A.A.: "High Resolution CAT Imaging of Fractures in Consolidated Materials," *Int. J. Rock Mech. Min. Sci*. (1997), 34 (3/4), 358-375.
18. He, M.: "Application of X-ray Tomography to Measurement of Fractures in Rocks," M.S. Thesis, Stanford University (1998).
19. Putra, E., Muralidharan, V., and Schechter, D.S.: "Overburden Pressure Affects Fracture Aperture and Fracture Permeability in a Fracture Reservoir," *SA Journal of Technology* (Fall 2003), pp 57-63.

Table 1.1 – Properties of Berea core

Core Properties	
Length	10.414 cm
Diameter	2.413 cm
Porosity	22.53%
Permeability	248 md

Table 1.2 – Oil Recovery Obtained at Different Injection Rates Using Distributed Fracture Aperture Model

	Inj rate, cc/min	Oil recovery, %IOIP
mean = 138.6 μm σ = 150.3	0.2	69.77633588
	0.5	69.04828244
	0.8	68.37442748
mean = 157.4 μm σ = 162.4	0.2	69.5019084
	0.5	68.5240458
	0.8	67.75658397
mean = 198 μm σ = 172.6	0.2	68.9879771
	0.5	67.64169847
	0.8	66.51412214
mean = 370.5 μm σ = 211.8	0.2	68.48177481
	0.5	66.69589695
	0.8	64.69914122

Table 1.3 – Oil Recovery Obtained at Different Injection Rates Using Smooth Fracture Aperture (Parallel Plate) Model

	Inj rate, cc/min	Oil recovery, %IOIP
mean = 138.6 μm	0.2	68.17461832
	0.5	66.08416031
	0.8	64.28244275
mean = 157.4 μm	0.2	68.18568702
	0.5	65.83969466
	0.8	63.74045802
mean = 198 μm	0.2	68.08778626
	0.5	65.62977099
	0.8	63.07251908
mean = 370.5 μm	0.2	67.90076336
	0.5	65.36259542
	0.8	62.21374046

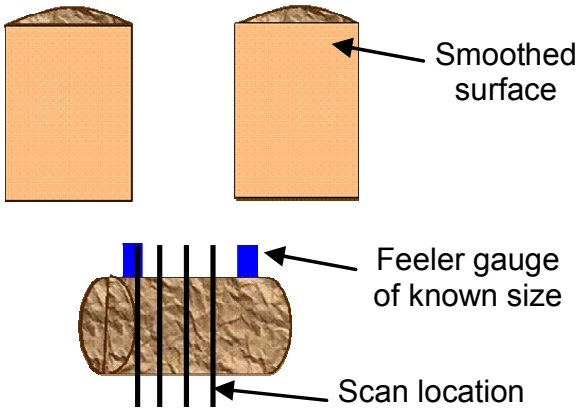

Fig. 1.1 – Experimental procedure showing feeler gauges and scan locations

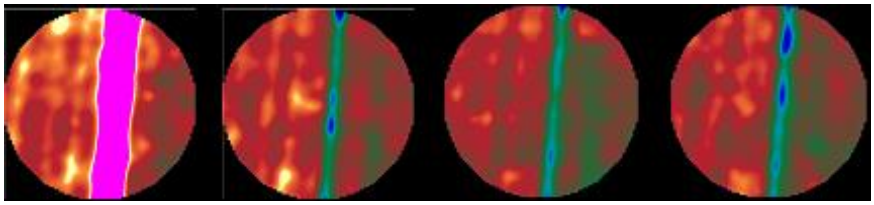

A. 38 µm feeler gauge

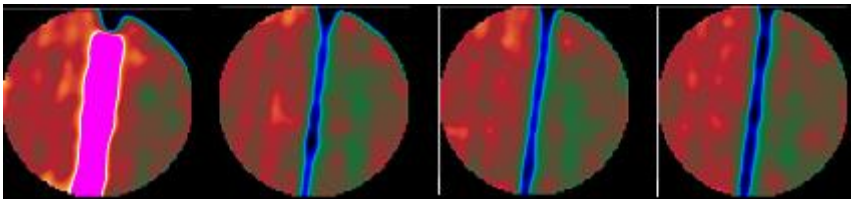

B. 102 µm feeler gauge

Fig. 1.2 – Scans taken along the length of the core for various feeler gauges

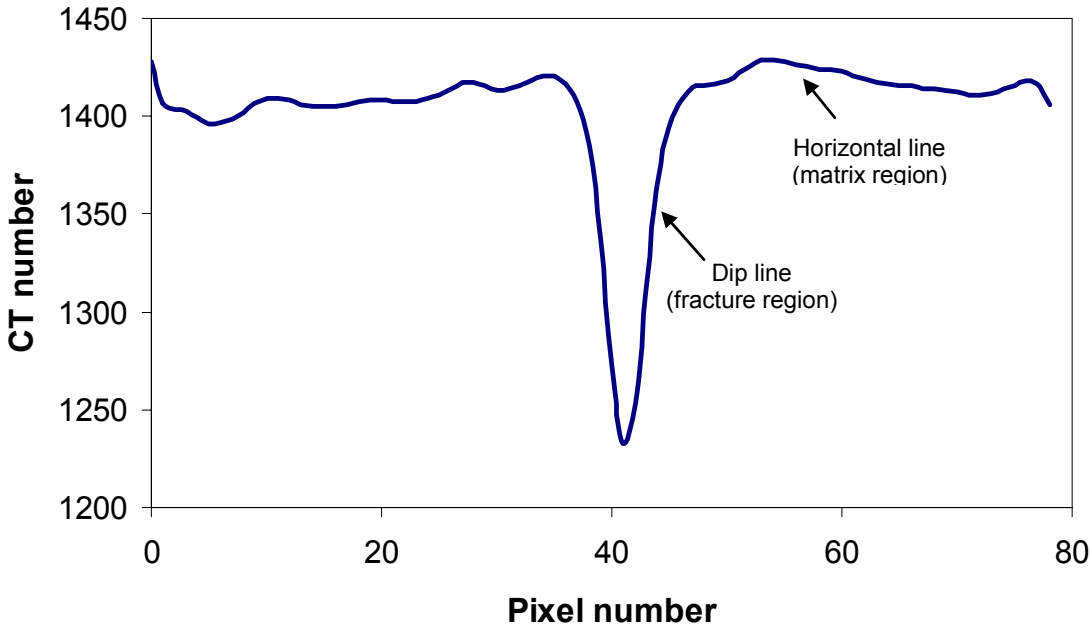

Fig. 1.3 – Average CT number plot for 38 μm feeler gauge

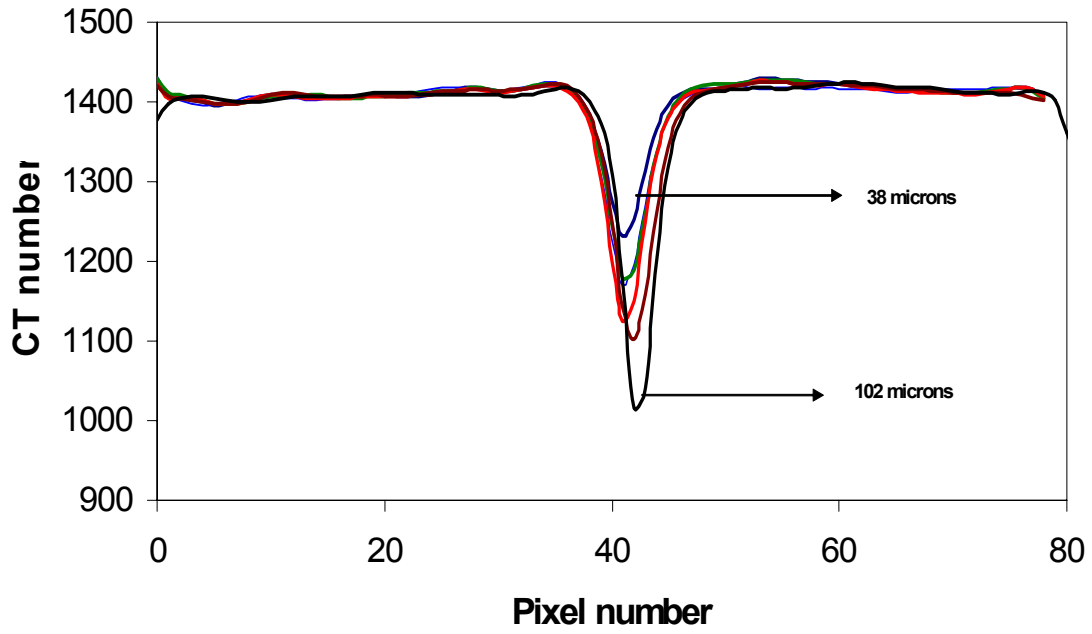

Fig. 1.4 – Comparison of CT number plots for different fracture sizes

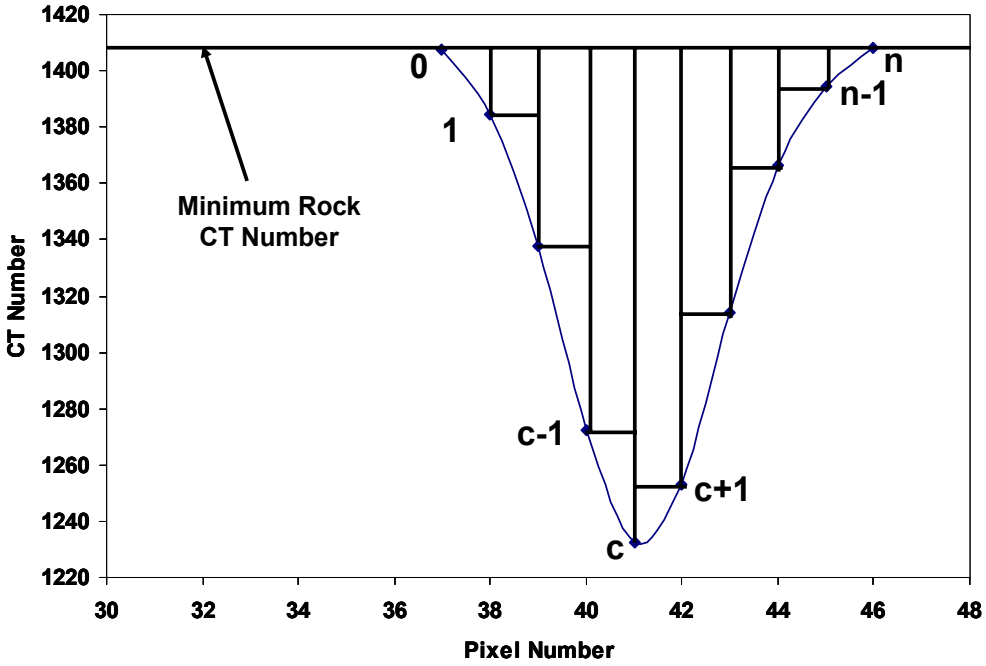

Fig. 1.5 – Integrated area in the fracture region showing the index of integrated CT

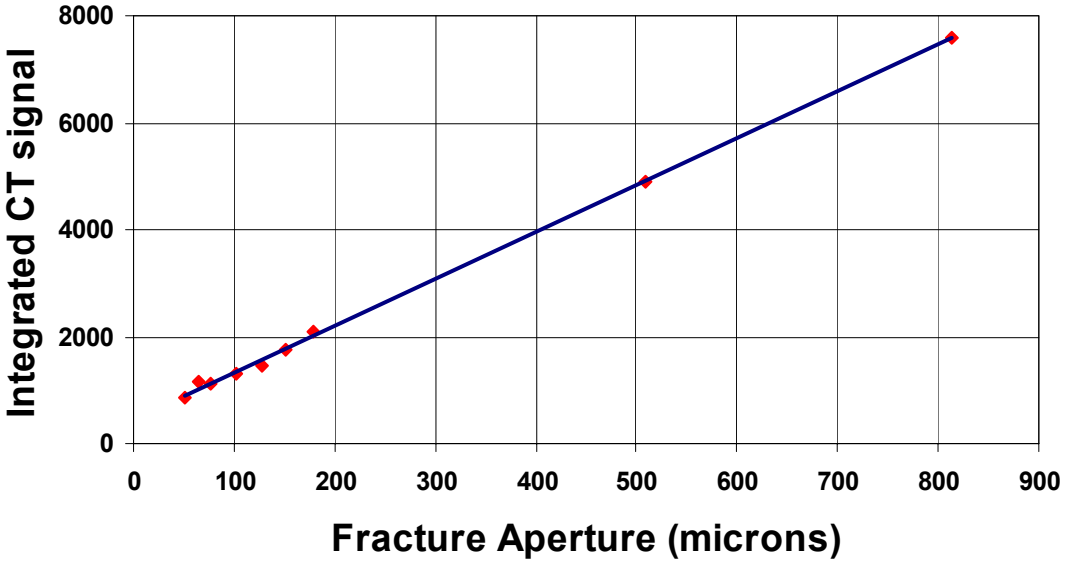

Fig. 1.6 – Calibration curve between integrated CT signal and fracture aperture

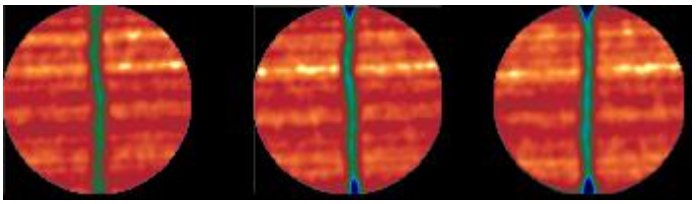

A. No overburden pressure

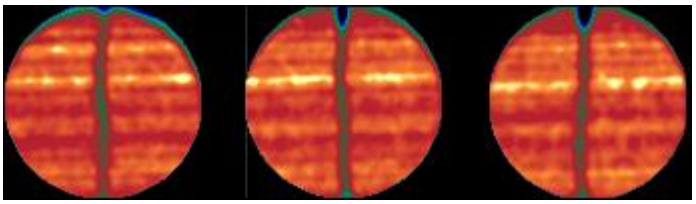

B. 500 psi overburden pressure

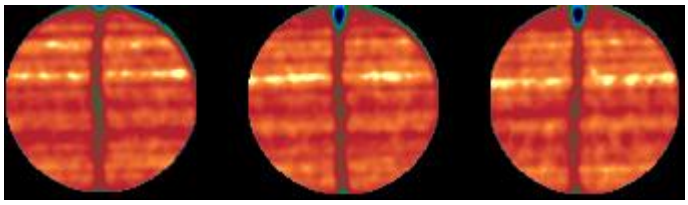

C. 1000 psi overburden pressure

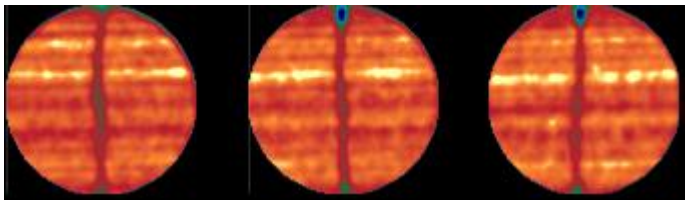

D. 1500 psi overburden pressure

Fig. 1.7 – Sample scans taken along the length of the core with different overburden pressures

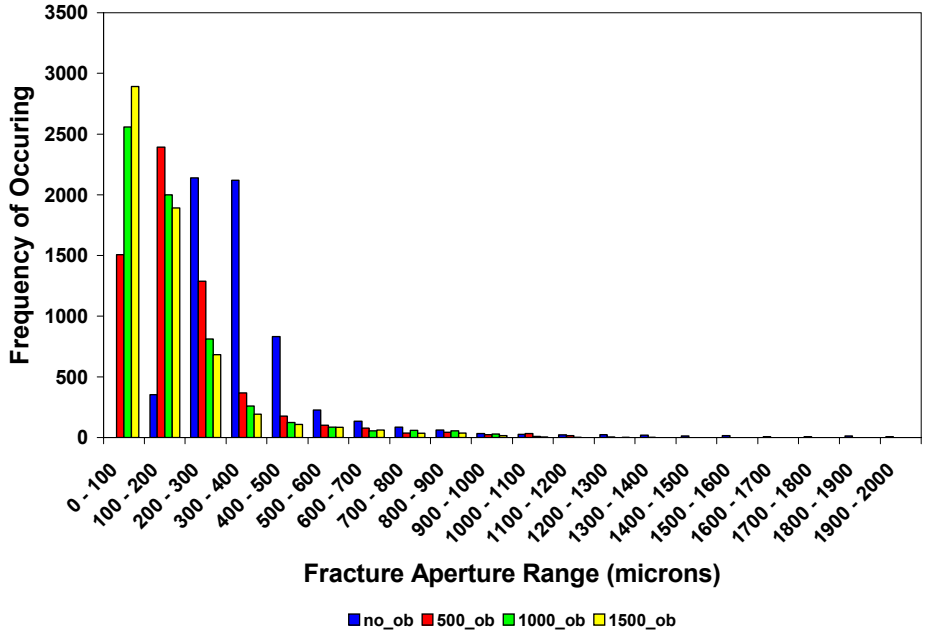

Fig. 1.8 – Comparative study of fracture aperture distribution under various overburden pressures

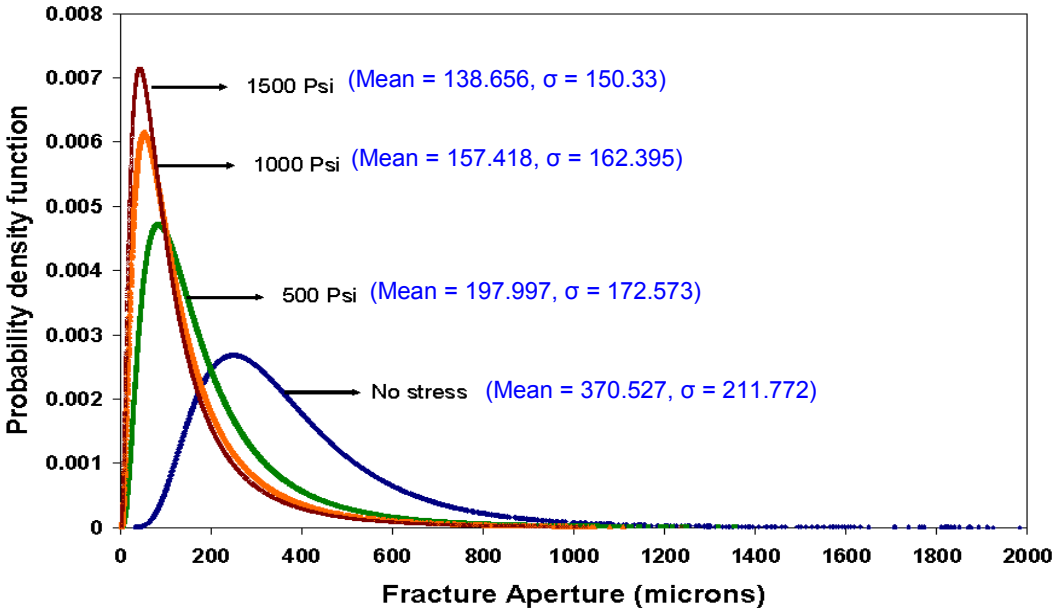

Fig. 1.9 – Comparison of aperture distribution curves for various overburden pressures

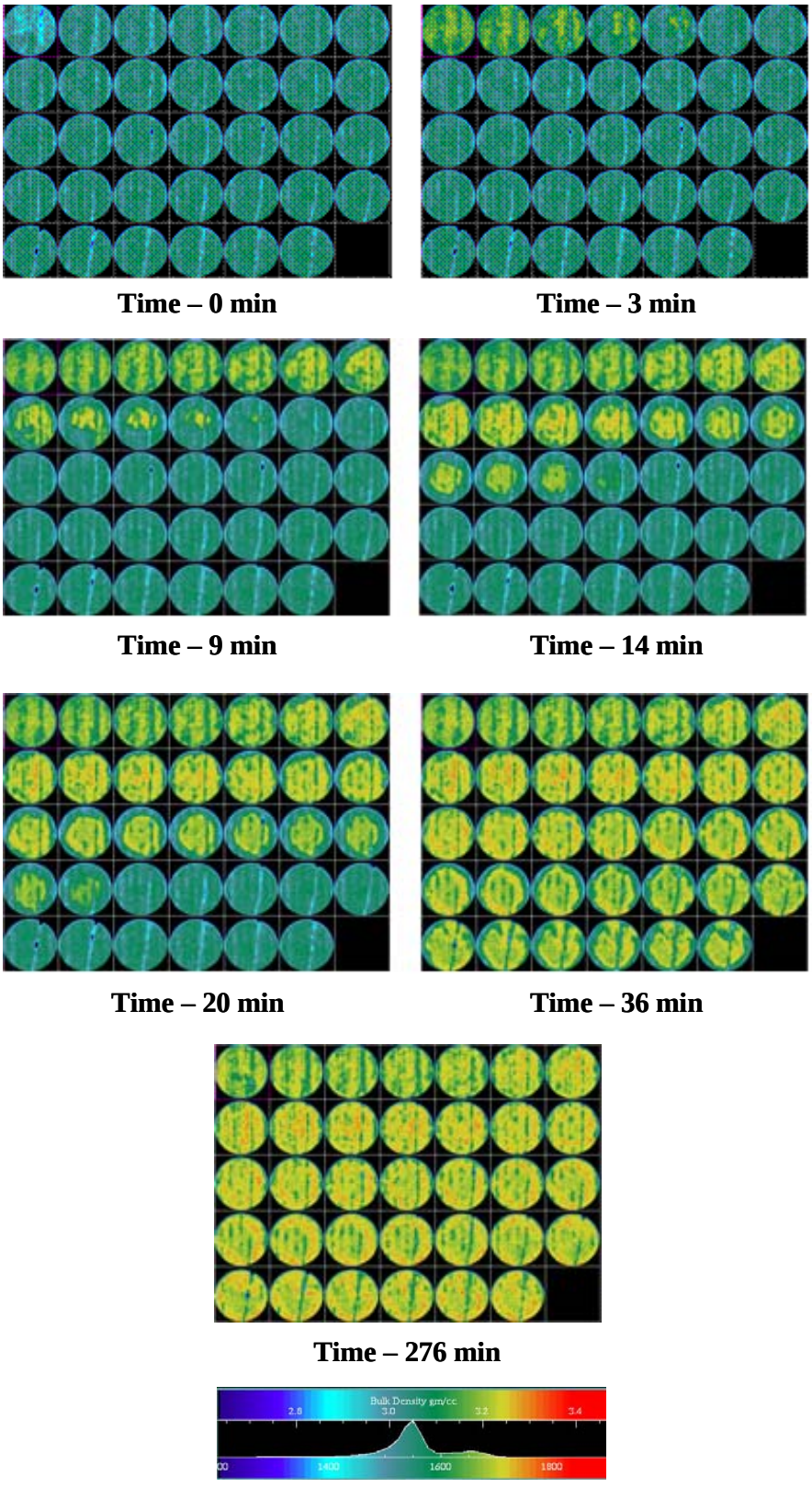

Fig. 1.10 – CT scan images during waterflooding at various timesteps

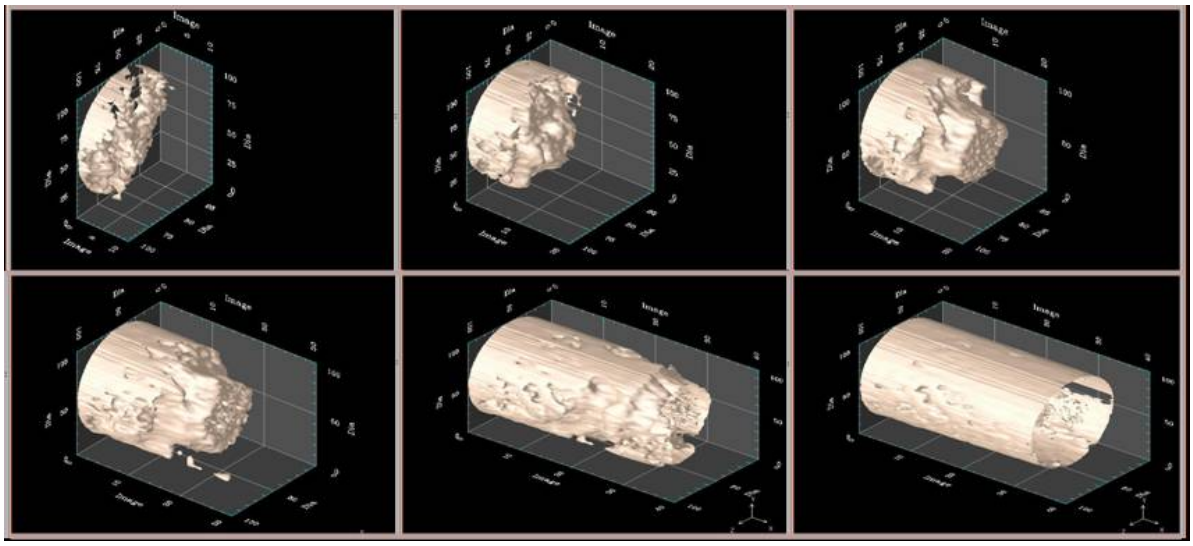

Fig. 1.11 – 3D images of water saturation during waterflooding at various timesteps

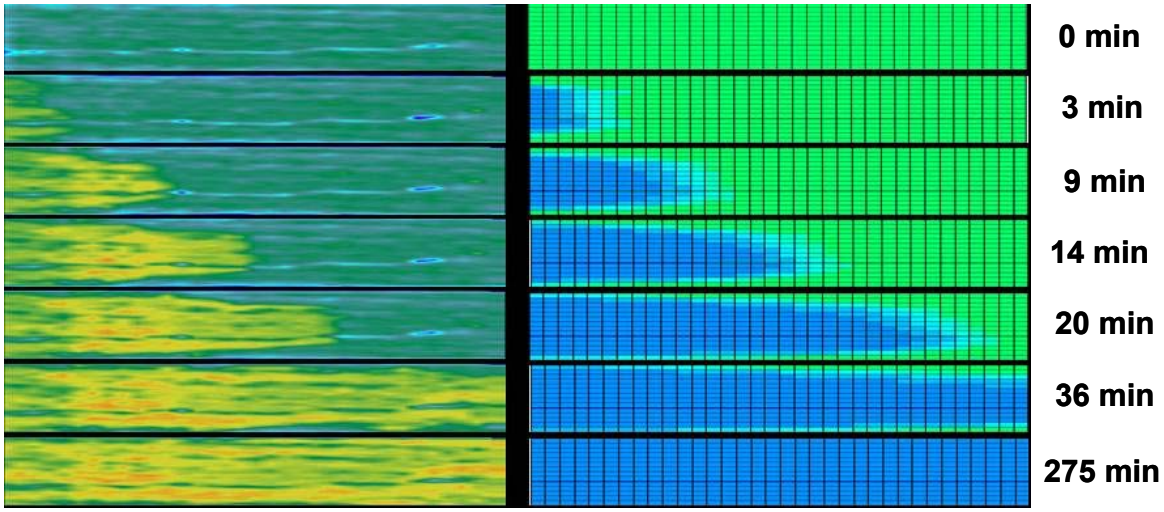

Fig. 1.12 – Comparison between CT and simulated water progression using parallel plate model

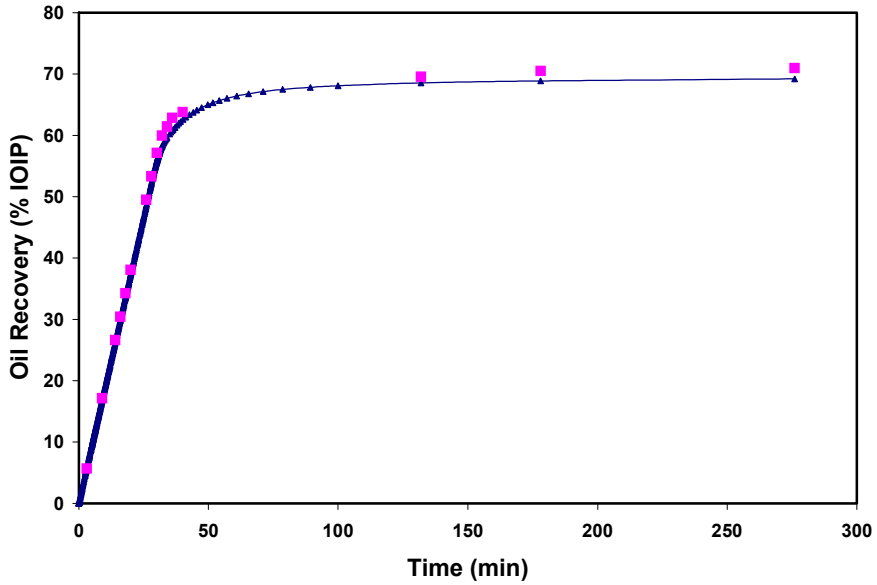

Fig. 1.13 – Comparison between observed and simulated oil recovery using parallel plate model

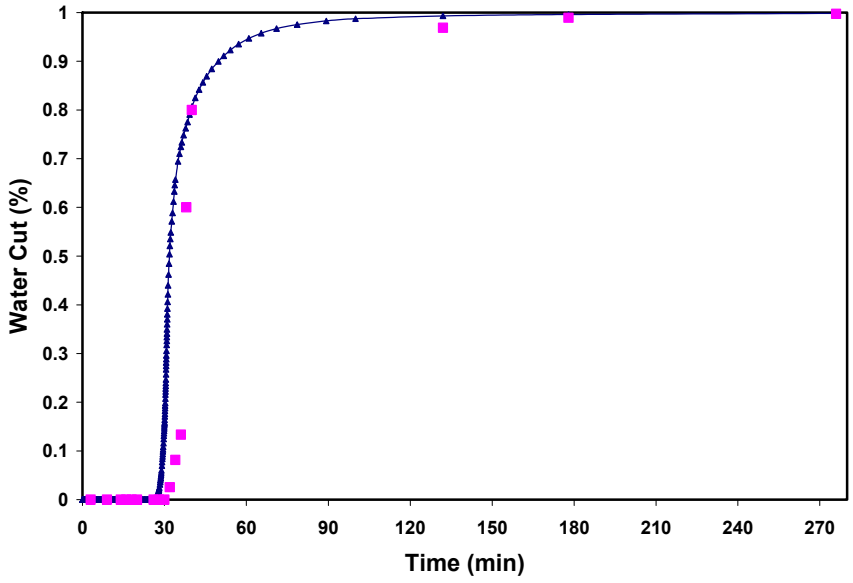

Fig. 1.14 – Comparison between observed and simulated water cut using parallel plate model

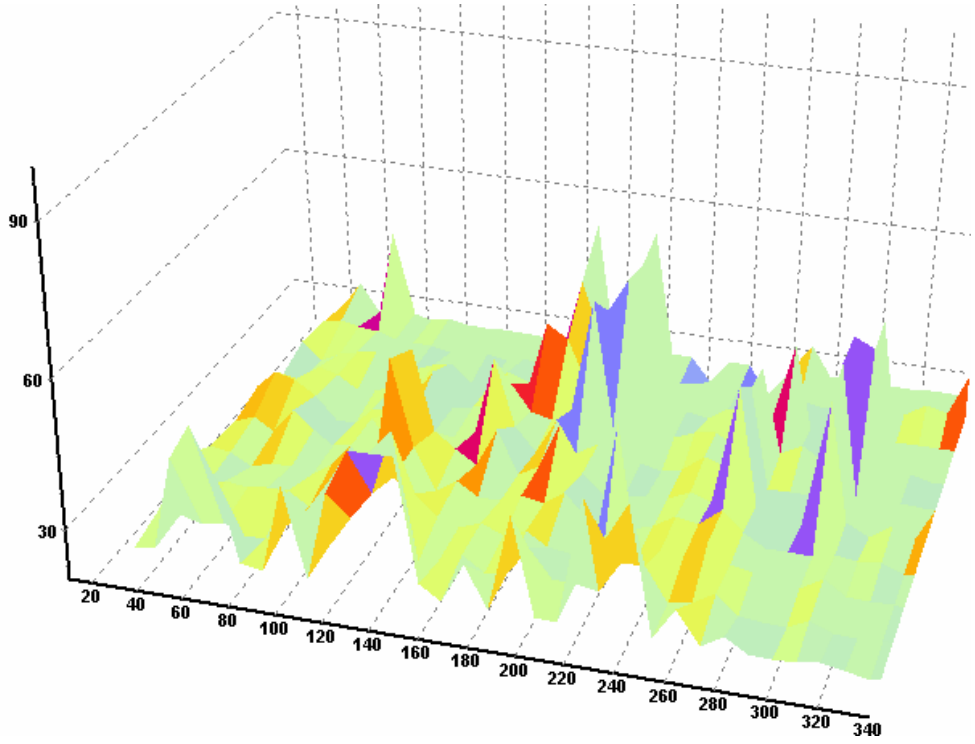

Fig. 1.15 – 3D map of aperture distribution

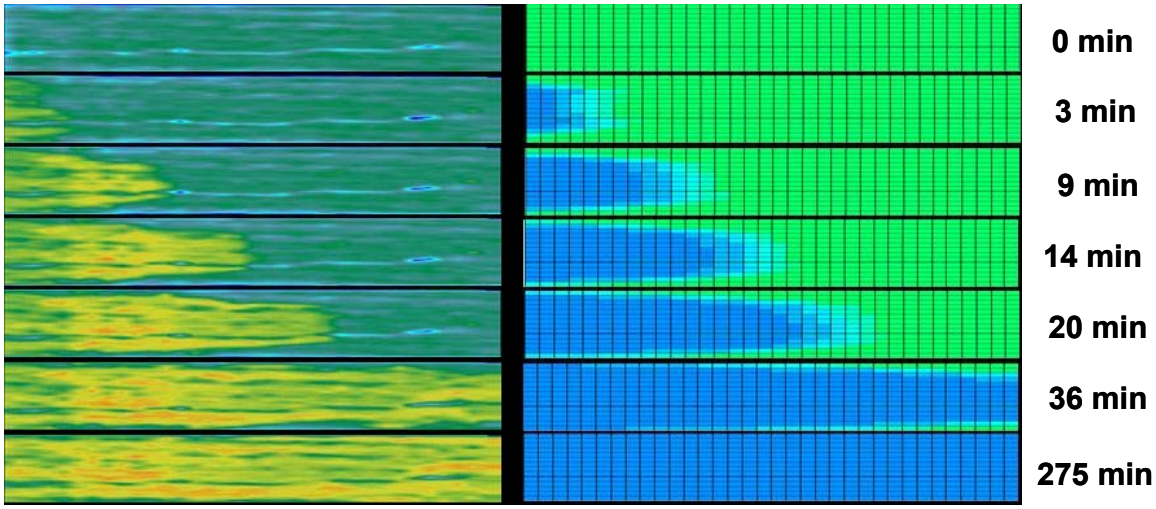

Fig. 1.16 – Comparison between CT and simulated water progression using distributed aperture model

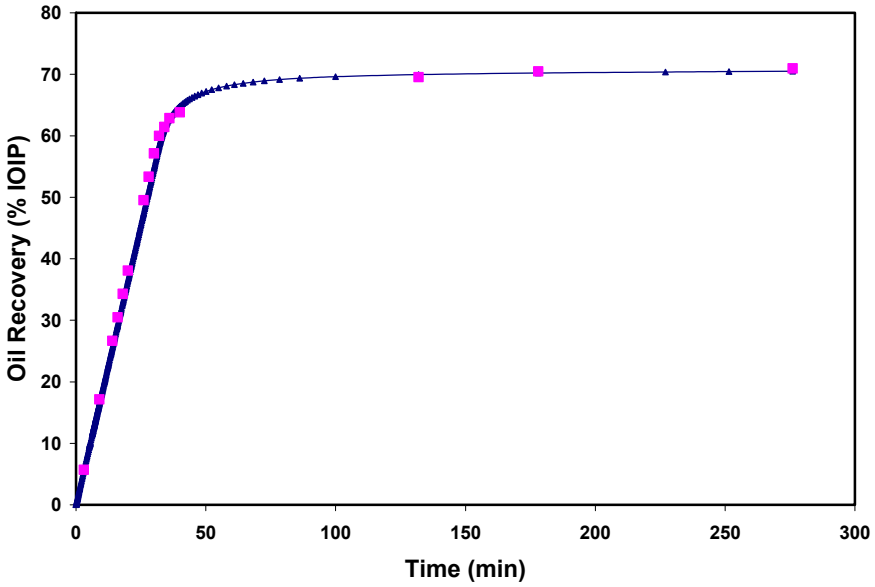

Fig. 1.17 – Comparison between observed and simulated oil recovery using distributed aperture model

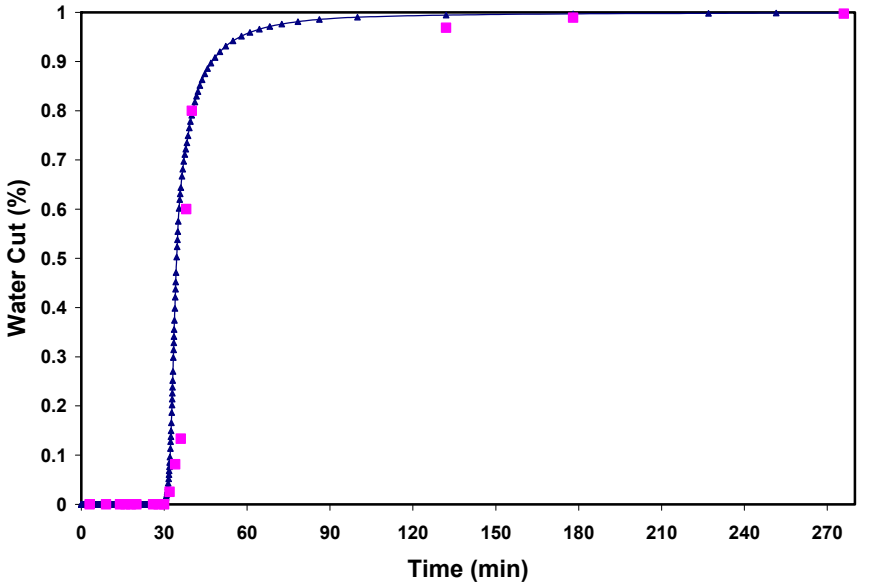

Fig. 1.18 – Comparison between observed and simulated water cut using distributed aperture model

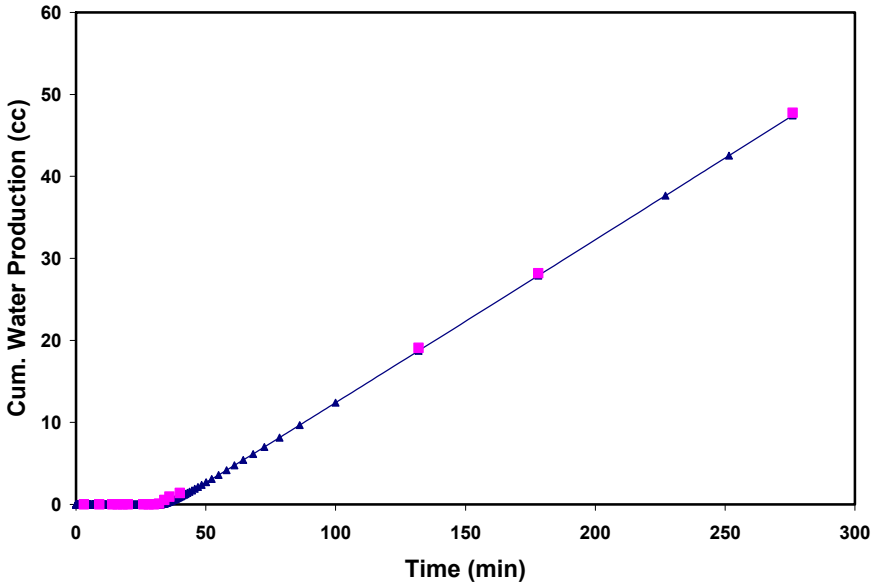

Fig. 1.19 – Comparison between observed and simulated cumulative water production using distributed aperture model

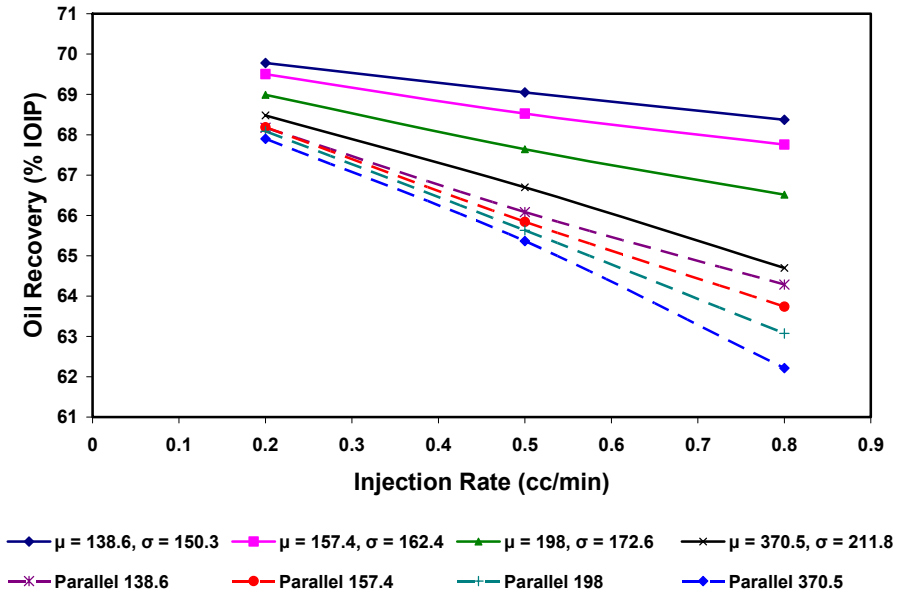

Fig. 1.20 – Sensitivity of oil recovery to fracture aperture size, distribution, and injection rates

Chapter II

A Unique Grid-Block System for Improved Grid Orientation

2.1 Introduction

It has been demonstrated by several authors[1-5] that two-dimensional simulations of immiscible displacements with unfavorable mobility ratio exhibit grid orientation effect. In fact, despite the fact that the reservoir is isotropic and homogeneous with favorable mobility ratio, there can still be an effect of grid orientation. To examine this effect, we conducted simulations of a quarter five-spot waterflood using parallel and diagonal grid systems, as illustrated in **Fig. 2.1.** A parallel grid system is a grid that is oriented parallel to injector-producer pairs. Meanwhile, a diagonal grid system is a grid oriented at 45° between injector and producer pairs. The distance of a producer to an injector and the size of the grid blocks are the same for both grid systems. Waterflood simulations were performed for oil/water mobility ratios (M) of 0.5, 1.0 and 10. The input data and the grid sizes are shown in **Tables 2.1 and 2.2.**

Since the distance of injector to producer is the same, we expect to get similar recovery performance from both grid systems. However, when we compare the recovery performance of parallel grid blocks of 8x8 and diagonal of 6x6, the recovery performances from both grid blocks are different as seen in **Fig. 2.2**. This is because rotation of the coordinate axes results in differing amounts of truncation error.[11] Increasing the resolution of grid blocks may reduce truncation error and lessen dispersion for a favorable mobility ratio (M<1.0) as pointed out by previous authors.

Thus, we increased the number of grid blocks in diagonal and parallel grid blocks at M = 0.5. We found that recovery performance is not sensitive to the number of diagonal grid blocks in the model (**Fig. 2.3**). However, as the number of the parallel grid blocks is increased, the recovery performance changes gradually until it converges to a single recovery curve (**Fig. 2.4)**. The recovery performances of finer grid blocks in both models (diagonal 21x21 vs. parallel 29x29), were compared. We found that the grid orientation effect was minimized (**Fig. 2.5**), as compared to those results from a parallel 8x8 and

diagonal 6x6 grid blocks. The saturation distribution map at VP_{inj} = 1.0 (**Fig. 2.6)** shows similar front profile of both parallel and diagonal grids indicating that the grid orientation effect is at its minimal.

However, at M=1.0, the recovery performances in diagonal grid appears to be more sensitive to the number of grid blocks than those in parallel grid model as shown in **Fig. 2.7**. The sweep efficiency decreases gradually as the number of grid blocks are increased. As for the parallel grid, once again, the recovery performance converges at 15x15 number of grid blocks and higher, as shown in **Fig. 2.8**. The results for both the diagonal and parallel grid show a close agreement when the grid block numbers are at 57x57 and 41x41 for the parallel and diagonal grid models, respectively, finer than those grid block requirement at M=0.5 (**Fig. 2.9**).

As the mobility ratio is increased to M=10.0, the performance of the diagonal grid does not follow a certain trend, and therefore, lose its reliability (**Fig. 2.10**). On the other hand, for a parallel grid, the solution does not seem to converge even when a large number of grid blocks were used, as seen in **Fig. 2.11**. The saturation map for diagonal grid model shows viscous fingering at the saturation front while the parallel model also shows a distorted front (**Fig. 2.12**).

Based on this study, we can conclude that grid refinement can help to minimize the grid orientation effect when we have favorable mobility ratios, i.e. at M=1.0 or less. However, at an unfavorable mobility ratio, neither the parallel, diagonal grid orientation, nor grid refinement is effective in reducing the grid orientation effect.

Therefore, the purpose of this study is to propose a possible alternative method to reduce the grid orientation effect.

2.2 Literature Review

Several methods have been proposed to reduce the grid orientation effect throughout the years. Due to the vast amount of literature, we will not attempt to cover all of it here. Nonetheless, the literature can be divided into several major groups in terms of the approach taken to minimize the grid orientation effect.

Grid orientation effect in reservoir simulation caused by conventional rectangular 5-

point discretization scheme was reported by Todd. et. al.[1] They proposed the use of two-point upstream mobility weighting in replace of the generally used single-point approximation. Meanwhile, a generalization of upstream weighting was proposed by Frauenthal et. al.[2], which involves using a weighting parameter between two mobilities instead of the simple single-point weighting. The main attraction of these techniques is that they can be easily implemented into existing computer codes and do not add significantly to computational time. However, based on the studies done by Vinsome and Au[9], they concluded that in an extreme case of unfavorable mobility ratio, the upstream formulation predicts a pressure drop across a shock front that is much smaller than it is supposed to be, and vice versa in the case of favorable mobility ratio.

The second group of the literature developed around the method of using a nine-point finite difference discretization scheme, which was initially proposed by Yanosik and McCracken[3]. This scheme is based on adding diagonal transmissibilities in the areal (X-Y) direction in order to reduce grid orientation effects when the flow is not aligned with the grid. Various forms of nine-point schemes were also introduced by subsequent authors[4-9]. Ko and Au[4] concluded that the nine-point scheme proposed by Yanosik and McCracken could not solve the problem of grid orientation for all mobility ratios since the weighting factor used in this method is a function of mobility ratio itself. In addition, as the nine-point scheme is a weighted-interpolation between the two five-point grids with a common center point and its diagonal transmissibilities, it hence lacks physical justification.

The third group concerns mainly with the numerical methods[11-14] - using a higher-order finite difference methods, or generally known as the high-order techniques (HOT). It is generally believed that the grid orientation effect is partly caused by numerical dispersion. For example, Pinto and Correa[13] as well as Wolcott et. al.[11] proposed using the Total Variation Diminishing (TVD) methods. Wolcott et. al.[11] used a combination of nine-point scheme and the third order Taylor's series expansion TVD scheme. It was reported than this method was able to reduce numerical dispersion and produce sharper saturation fronts.

On the other hand, Pruess and Bodvarsson[15] proposed the use of a seven-point discretization scheme, which is essentially a hexagonal grid-block model. They investigated steam injection problems with relatively coarse grids and concluded that the

hexagonal grid can reduce the grid orientation effect. The use of hexagonal grid was further supported by Heinemann et. al.[16] in their PEBI (Perpendicular-Bisector) grid model. They also reported the unrealistic saturation front produced by the hexagonal grid and by the Cartesian grid with the nine-point formulation for M = 50. Meanwhile, Hirasaki and O'Dell[17] as well as Robertson and Woo[18] were some of the earliest authors who proposed the use of orthogonal curvilinear grid for the simulation of pattern floods.

The current trend includes the development of flexible gridding to alleviate the problem associated with grid orientation effect from using rectangular Cartesian grid.

2.3 Hybrid Grid Block (HGB) Generation

In this paper, we propose the use of HGB to reduce grid orientation effect. In HGB, the rectangular grid blocks are interspersed with octagonal grid blocks. The boundaries are then populated with triangular grid blocks. Thus, the grid model consists of a "structured" grid block system. This arrangement is shown in **Fig. 2.13**. The basic elements are generated from input data, including the number of grid blocks and the interval length in each direction. Based on this predefined information, parameters such as the total grid blocks and the distance between each grid block can be calculated.

Since HGB assumes a block-centered geometry, transmissibility calculations are based upon the distances between the centroids of each grid block. Using **Fig. 2.14** as an example, Cell #1 is connected to Cell #3 "through" cross sectional area A_{13}. Its interface transmissibility can be calculated as shown in Eq. 2.1.

$$T_{13} = \frac{0.00633\, k\, A_{13}}{L_{13}} \quad \text{.....} \quad 2.1$$

The structure of the coefficient matrix depends on the dimensions of the problem and the ordering of the grid blocks. The objective of using different grid block-ordering schemes is to reduce the computational work involved in solving a linear equation of finite difference equations. Therefore, we should order the points in such a way that the bandwidth is the minimum possible to maximize the efficiency of the simulator. Using the HGB model, several numbering systems were tested. Considering a simple 25-block case,

Fig. 2.15 shows an example grid ordering and the corresponding matrix structures. A type of "diagonal count ordering" was used, where the grid blocks are numbered consecutively along the diagonals starting with the shortest direction as shown in **Fig. 2.15**. This method groups the blocks by "diagonal count", and increases as we move from the lower left through the grid to the upper right.

There are two general methods for solving the resulting linear equation – direct and iterative. In this case, the iterative method of preconditioned and stabilized biconjugate-gradient is chosen due to its versatility. In HGB, the coefficient matrix has a sparse structure, containing a large number of zero entries. Since only non-zero matrix elements are used, implementing sparse matrix solver using this method requires relatively small memory storage.

Palagi[19] presented an analytical well model based on Peaceman's[20] work on well modeling for rectangular grid blocks which can be applied to grids of any geometry. In HGB grid, this well model is adopted for wells placed in center of the regular octagonal grid blocks, such as shown in **Fig. 2.16**. Eq. 2.2 describes how the effective wellbore radius term, r_o, is calculated.

$$r_o = d_{ij} \exp\left(\frac{2\pi}{N(b/d)_{ij}} \right) \quad \text{..... 2.2}$$

2.4 Discussion of Results

To test the viability of the HGB grid, a two-dimensional IMPES simulator was developed and HGB is incorporated. The simulator is then validated with GeoQuest's Eclipse 100™ 2003A. Single-point upstream weighting of mobility was used. Since the HGB grid cannot be validated "directly" with any commercial simulators to the best of the authors' knowledge, the Cartesian grid model in the simulator is validated with rectangular grid models. **Fig. 2.17** shows the results of one of the validation cases that were run. This particular example is for the case of a two-dimensional areal model of a water-oil primary depletion of an undersaturated reservoir with one injector and one producer. Once the algorithm is validated, it is then applied to the HGB grid.

One quarter five-spot pattern model were chosen to run a two-well, diagonal grid (85 grid blocks) and a four-well, parallel grid (145 grid blocks), as shown in **Fig. 2.18**. Different mobility ratios of 1.0, 10.0 and 50.0 were used in these cases respectively. The data used in these runs are shown in **Table 2.3**.

From **Fig. 2.19**, we can see that the parallel and diagonal HGB grid model give very similar results for both favorable and unfavorable mobility ratios cases that were run. This is because flow can progress in several different directions in the octagonal grid blocks. The result is that the differences between the parallel and diagonal orientation are greatly reduced. Even so, the discrepancies between these two grids in HGB (with relative difference of approximately 6%) are negligible and believed to be caused by the presence of the square grid blocks.

The HGB grid is shown to be effective in reducing the grid orientation effect in displacements with unfavorable mobility ratios. From the saturation distribution map as shown in **Figs. 2.20-2.21**, we can see that the predictions are more realistic than the fingering profile produced by the Cartesian grids shown earlier in **Fig. 2.12**. HGB produces a "smoother" saturation front and therefore, the smaller mobility ratio (M=1.0) predicts a higher sweep efficiency.

From **Figs. 2.20-2.21**, we can see that the front movement is faster when the mobility ratio increases. This is due to the fact that the displacing fluid is moving at a much higher velocity than oil, the displaced fluid. Fingering of the displacing fluid also results in faster breakthrough times.

In addition, a closer agreement between the parallel and diagonal grid does not mean that the results give true values. Further studies should be done to investigate the accuracy of these results. Without an analytical solution, no definite conclusions can be drawn regarding the accuracy of the finite difference solutions.

Furthermore, we have seen that besides the orientation of the grid, the mobility ratios and the grid block sizes, the inherent numerical method used in the formulation of the solutions would certainly contribute to the problem of grid orientation effect. As Brand et. al.[21] stated in their paper, "When the grid is refined, the solution still depends on the size and orientation of the underlying grid, as long as numerical diffusion dominates over

physical dispersion and diffusion." When this occurs, the quantitative interpretation of the simulation results would be difficult. Perhaps the best way is to combine all the solutions method, i.e. using a grid where flow can easily progress to any direction, and applying methods to reduce the numerical dispersion effect in the underlying grid.

2.5 Conclusions

1. Grid orientation effect was observed in rectangular Cartesian grid models even at isotropic and homogeneous reservoir with favorable mobility ratio.
2. Grid refinement can help to minimize the grid orientation effect in rectangular Cartesian grid models when there are favorable mobility ratios, ie. M=1.0 or less. However, at an unfavorable mobility ratio, neither the parallel, diagonal grid orientation, nor grid refinement is effective in reducing the grid orientation effect.
3. HGB grid is able to minimize the grid orientation effect even for unfavorable mobility ratio displacement problems, with relative difference of about 6% for all the cases run.

Nomenclature

M = Mobility ratio

k = absolute permeability

k'_r = end-point relative permeability

S = saturation

Δx = size of block in x-direction

Δy = size of block in y-direction

μ = viscosity

ϕ = porosity

A = cross-sectional area

T = transmissibility

L = length between two adjacent centroids

r_o = effective wellbore radius

θ_{ij} = 2π for a well located in the center of the block

i = center of grid block containing the well

j = center of grid block that is neighbor of well block i

b_{ij} = length of one equal side of polygon

d_{ij} = distance between the centers of neighboring grid blocks i and j

N = number of equal sides

VP = pore volume

Subscripts

inj = injection

o = oil

w = water

x = x-direction

y = y-direction

References

1. Todd, M.R., O'Dell, P.M. and Hirasaki, G.J.: "Methods for Increased Accuracy in Numerical Simulation", paper SPE 3516 presented at the 1971 46th Annual Fall Meeting, New Orleans, October 3-6.
2. Frauenthal, J.C., Rolaud, B. and Towler, B.F.: "Reduction of Grid-Orientation Effects in Reservoir Simulation with Generalized Upstream Weighting", paper SPE 11593 presented at the 1983 Symposium on Reservoir Simulation, San Francisco, November 15-18.
3. Yanosik, J.L. and McCracken, T.A.: "A Nine-Point, Finite-Difference Simulator for Realistic Prediction of Adverse Mobility Ratio Displacements", paper SPE 5734 presented at the 1976 4th SPE-AIME Symposium of Numerical Simulation of Reservoir Performance, Los Angeles, February 19-20.
4. Ko, S.C.M. and Au, A.D.K.:"A Weighted Nine-Point Finite-Difference Scheme for Eliminating the Grid Orientation Effect in Numerical Reservoir Simulation", paper SPE 8248 presented at the 1979 54th Annual Fall Meeting, Las Vegas, Nevada, September 23-26.
5. Coats, K.H. and Modine, A.D.: "A Consistent Method for Calculating Transmissibilities in Nine-Point Difference Equations", paper SPE 12248 presented at the 1983 Reservoir Simulation Symposium, San Francisco, November 15-18.

6. Shah, P.C.: "A Nine-Point Finite Difference Operator for Reduction of the Grid Orientation Effect," paper SPE 12251 presented at the 1983 Reservoir Simulation Symposium, San Francisco, November 15-18.
7. Ostebo, B. and Kazemi, H: "Mixed Five-Point/Nine-Point Finite-Difference Formulation of Multiphase Flow in Petroleum Reservoirs", paper SPE 21227 presented at the 1991 11th Reservoir Simulation Symposium, Anaheim, February 17-20.
8. Shiralkar, G.S. and Stephenson, R.E.: "A General Formulation for Simulating Physical Dispersion and a New Nine-Point Scheme", paper SPE 16975 presented at the 1987 62nd Annual Technical Conference and Exhibition, Dallas, September 27-30.
9. Vinsome, P.K. and Au A.K.: "One Approach to the Grid Orientation Problem in Reservoir Simulation," paper SPE 8247 presented at the 1979 54th Annual Fall Technical Conference and Exhibition of the Society of Petroleum Engineers of AIME, Los Angeles, September 23-26.
10. Brand, C.W., Heinemann, J.E., and Aziz, K.: "The Grid Orientation Effect in Reservoir Simulation", paper SPE 21228 presented at the 1991 11th Symposium on Reservoir Simulation, Anaheim, California, February 17-20.
11. Wolcott, D.S., Kazemi, H., and Dean, R.H.: "A Practical Method for Minimizing the Grid Orientation Effect in Reservoir Simulation", paper SPE 36723 presented at the 1996 Annual Technical Conference and Exhibition, Denver, October 6-9.
12. Shin, D. and Merchant, A.R.: "Higher-Order Flux Update Function Method for Reduction of Numerical Dispersion and Grid Orientation Effect in Reservoir Simulation", paper SPE 25600 presented at the 1993 Middle East Oil Technical Conference and Exhibition, Bahrain, April 3-6.
13. Pinto A.C.C. and Correa, A.C.F.: "High-Resolution Schemes for Conservation Laws: Applications to Reservoir Engineering," paper SPE 24262 presented at the 1992 European Petroleum Computer Conference, Stavanger, Norway, May 25-27.
14. Chen, W.H. and Durlofsky, L.J.: "Minimization of Grid Orientation Effects Through Use of Higher-Order Finite Difference Methods", paper SPE 22887 presented at the 1991 66th Annual technical Conference and Exhibition, Dallas, October 6-9.
15. Pruess, K. and Bodvarsson, G.S.: "A Seven-Point Finite Difference Method for Improved Grid Orientation Performance in Pattern Steamfloods," paper SPE 12252

presented at the 1983 Reservoir Simulation Symposium, San Francisco, November 15-18.

16. Heinemann, Z. E. and Brand, C.W.: "Modeling Reservoir Geometry with Irregular Grids", paper 18412 presented at the 1989 10th SPE Symposium on Reservoir Simulation, Houston, TX, February 6-8.
17. Hirasaki, G.J. and O'Dell, P.M.: "Representation of Reservoir Geometry for Reservoir Simulation," Reprint Series No. 11 – Numerical Simulation, Society of Petroleum Engineers of AIME, Dallas (1973) 157-168.
18. Robertson, G.E. and Woo, P.T.: "Grid-Orientation Effects and the Use of Orthogonal Curvilinear Coordinates in Reservoir Simulation", paper SPE 6100 presented at the SPE-AIME 51st Annual Fall Technical Conference and Exhibition, New Orleans, October 3-6.
19. Palagi, C.L.: "Generation and Application of Voronoi Grid to Model Flow in Heterogeneous Reservoirs", Ph.D. Dissertation, Stanford University, May 1992.
20. Peaceman, D.W.: "Interpretation of Well-Block Pressures in Numerical Reservoir Simulation", paper SPE 6893 presented at the 1977 52nd SPE-AIME Annual Fall Technical Conference and Exhibition held in Denver, 9-12 Oct.
21. Brand, C.W., Heinemann, J.E., and Aziz, K.: "The Grid Orientation Effect in Reservoir Simulation", paper SPE 21228 presented at the 1991 11th SPE Symposium on Reservoir Simulation, Anaheim, California, February 17-20.

Table 2.1 – Data Used for Five-Spot Pattern Simulations

Parameter	**Value**
Rock Permeability, k	100 mD
Porosity, ϕ	0.20
Net Pay Thickness	10 ft
Production Rate, Q_o	18 STB/D
Injection Rate, Q_w	18 STB/D
Initial Water Saturation	0
Residual Oil Saturation	0
Initial Pressure	5000 psi
Area of Reservoir (Parallel)	20 acres
Area of Reservoir (Diagonal)	10 acres
Relative Permeability	$k_{rw} = \frac{S_w^{\,2}}{M(1-S_w^{\,2})+S_w^{\,2}}$ $k_{ro} = 1 - k_{rw}$ $M = \frac{k'_{rw}/\mu_w}{k'_{ro}/\mu_o}$

Table 2.2 - Grid Sizes Used in Cartesian Grid Models

Diagonal Grid	Grid Block Size ($\Delta x/\Delta y$)	Parallel Grid	Grid Block Size ($\Delta x/\Delta y$)
6 x 6	132 ft	8 x 8	133.34 ft
11 x 11	66 ft	15 x 15	66.7 ft
21 x 21	33 ft	29 x 29	33.355 ft
41 x 41	16.5 ft	57 x 57	16.668 ft

Table 2.3 - Data Used for HGB Pattern Simulations

Parameter	Value
Rock Permeability, k	100 mD
Porosity, ϕ	0.20
Net Pay Thickness	10 ft
Producer-Injector Distance	825 ft
Production Rate, Q_o	18 STB/D
Injection Rate, Q_w	18 STB/D
Initial Water Saturation	0.20
Residual Oil Saturation	0.20
Initial Pressure	5000 psi
Area of Reservoir (Parallel)	15 acres
Area of Reservoir (Diagonal)	7.5 acres

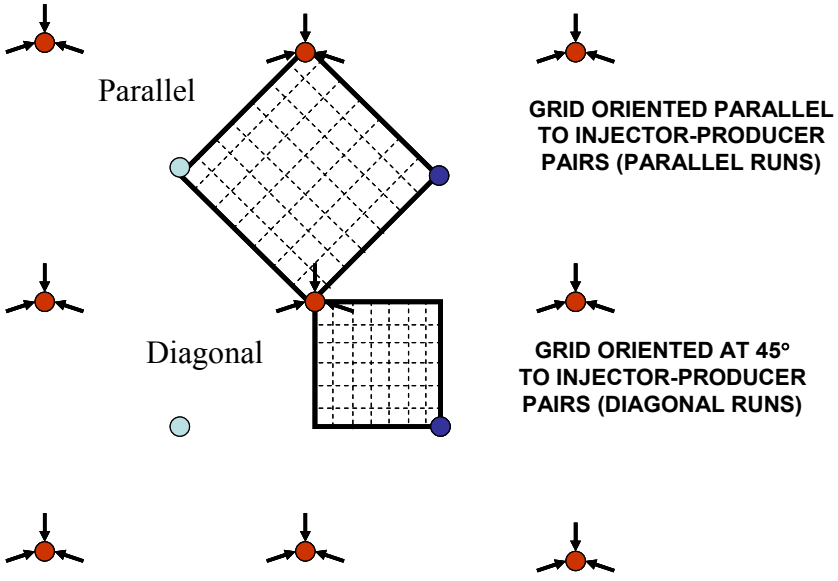

Fig. 2.1 – Parallel and diagonal orientation for simulations of waterflooding in five-spot symmetry elements (after Todd *et. al*).

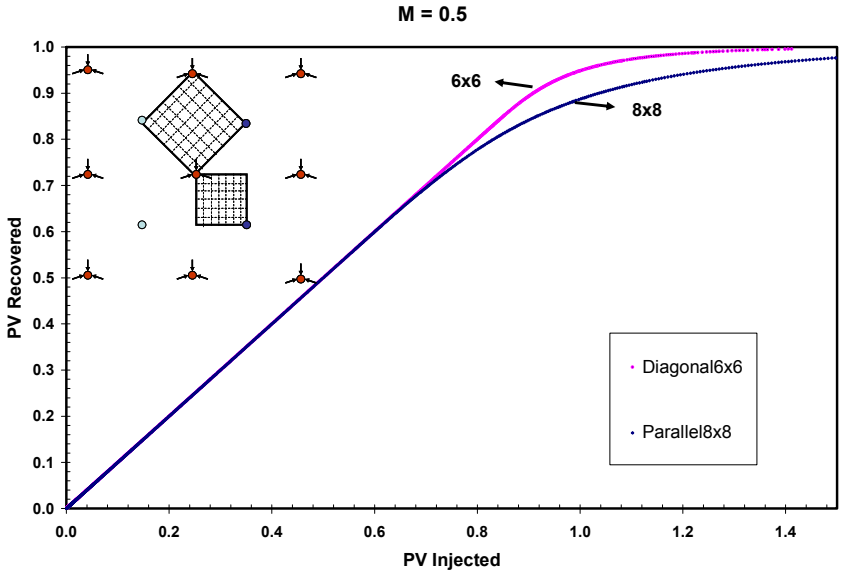

Fig. 2.2 – Predicted performance at *M*=0.5 for parallel (8x8) and diagonal (6x6) grid blocks.

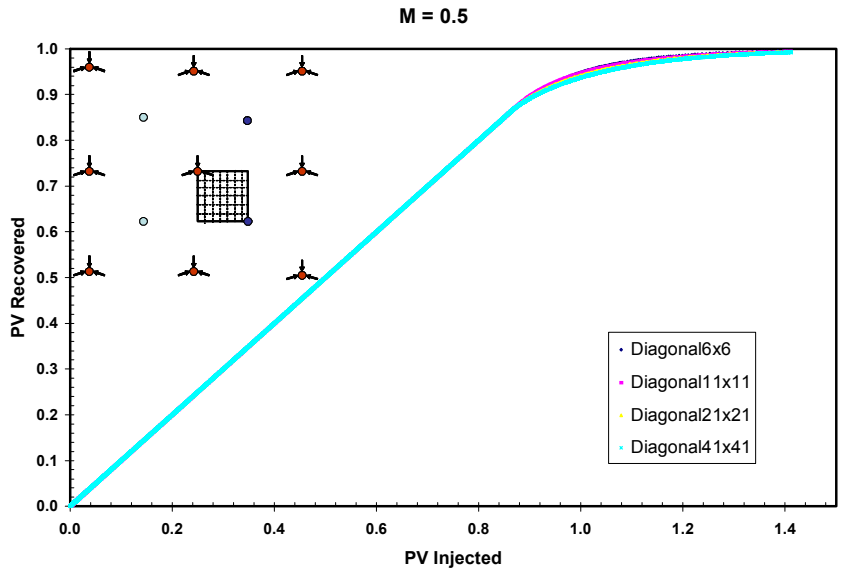

Fig. 2.3 – Predicted performance at *M*=0.5 for different number of diagonal grid blocks.

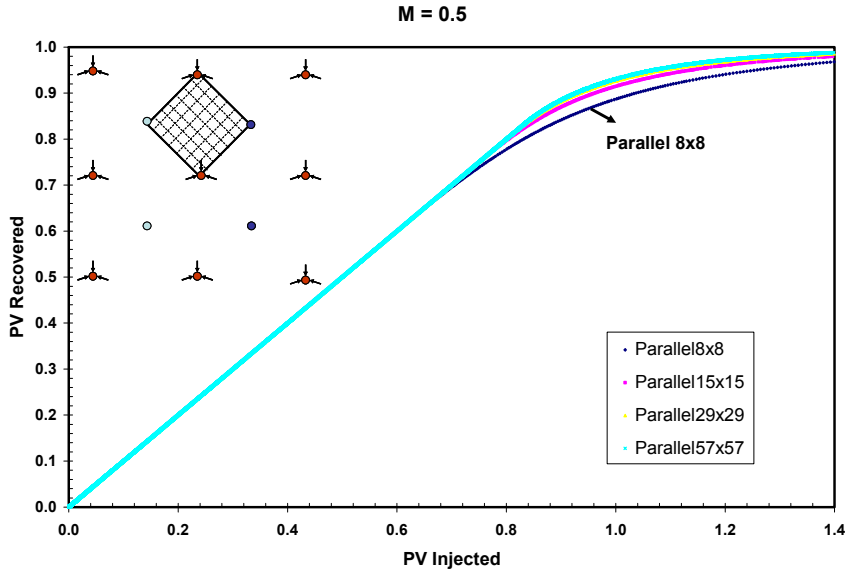

Fig. 2.4 – Predicted performance at *M*=0.5 for different number of parallel grid blocks.

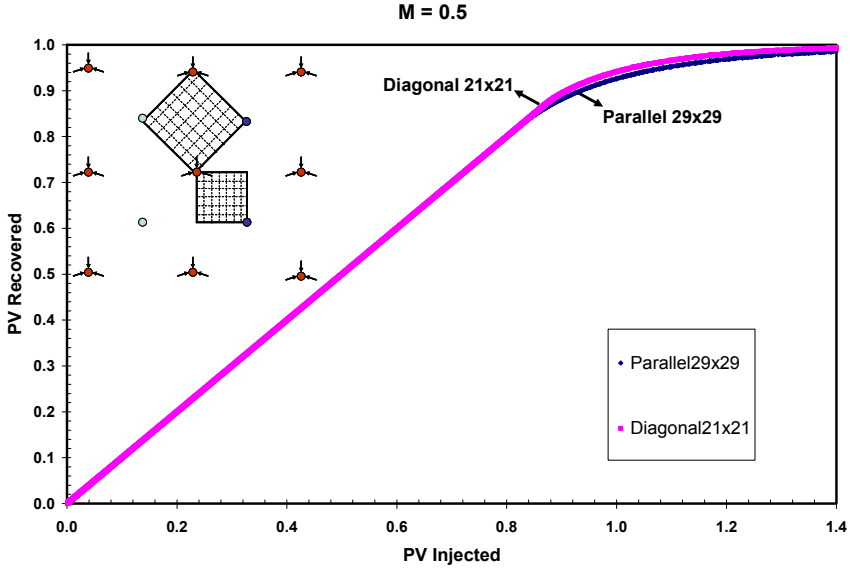

Fig. 2.5 – Predicted performance at *M*=0.5 for parallel (29x29) and diagonal (21x21) grid blocks.

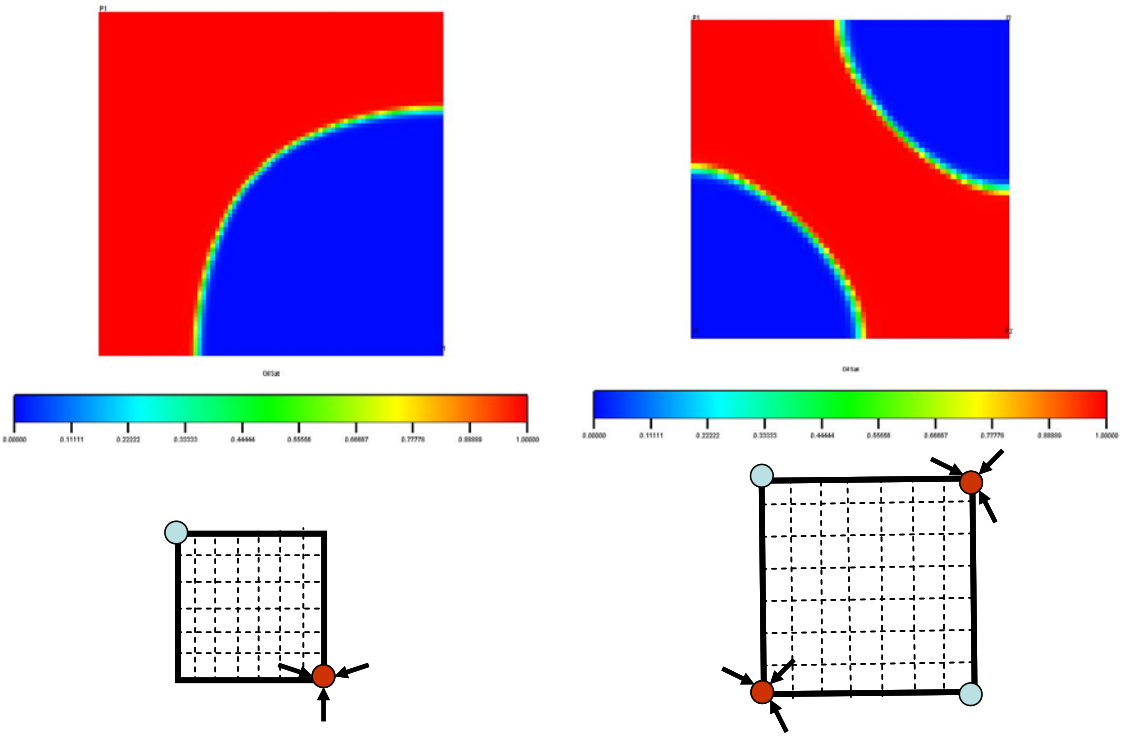

Fig. 2.6 – Saturation distribution map at *PVinj* =1.0 for *M*=0.5.

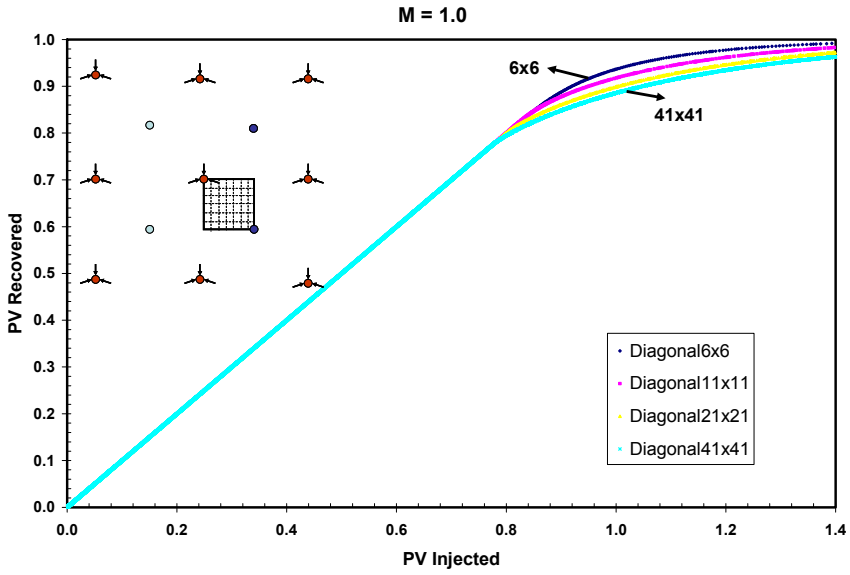

Fig. 2.7 – Predicted performance at *M*=1.0 for number of different diagonal grid blocks.

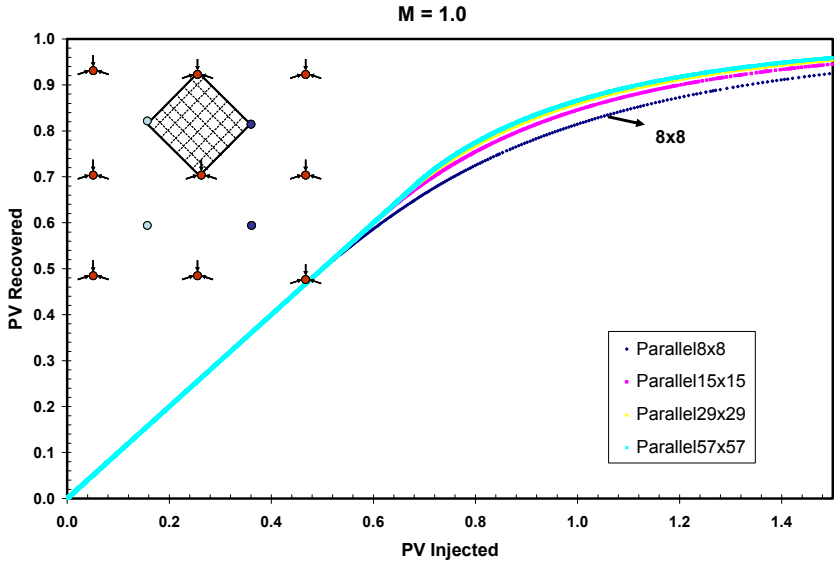

Fig. 2.8 – Predicted performance at *M*=1.0 for number of different parallel grid blocks.

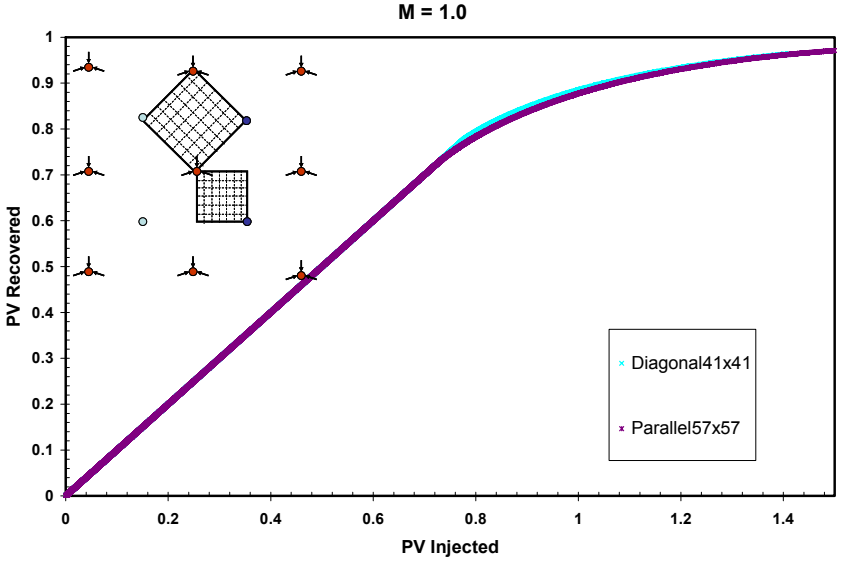

Fig. 2.9 – Predicted performance at *M*=1.0 for parallel (57x57) and diagonal (41x41) grid blocks.

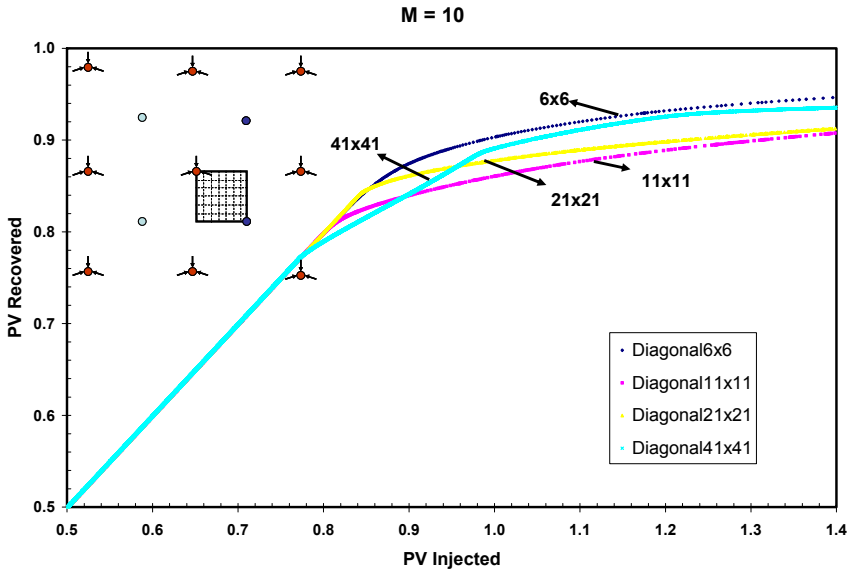

Fig. 2.10 – Predicted performance at *M*=10.0 for number of different diagonal grid blocks.

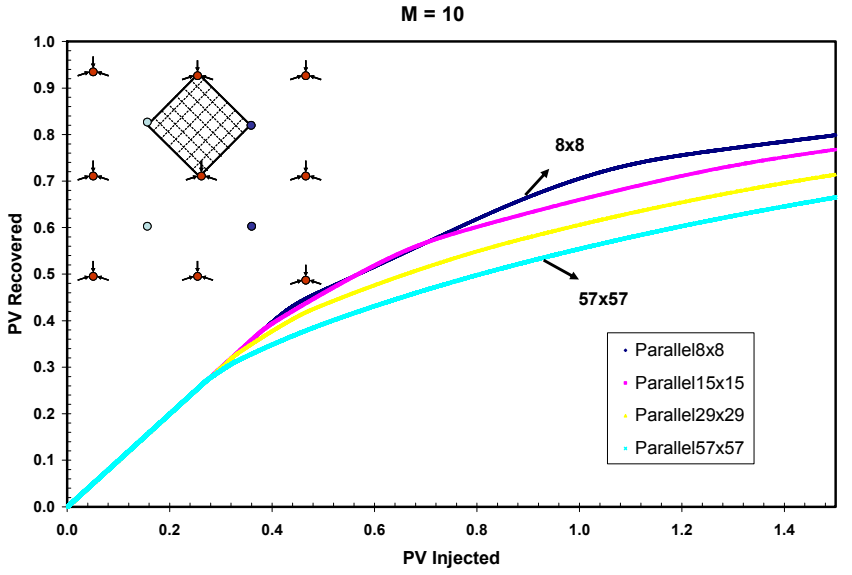

Fig. 2.11 – Predicted performance at *M*=10.0 for number of parallel grid blocks.

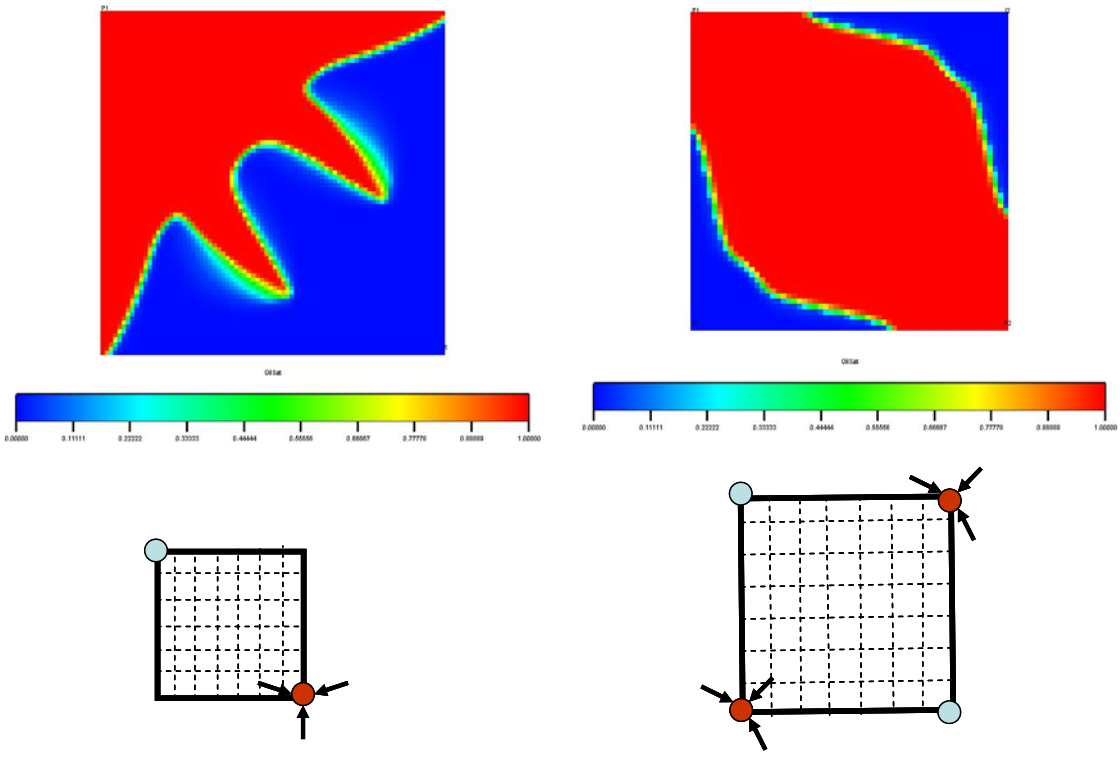

Fig. 2.12 – Saturation distribution map at *PVinj* =1.0 for *M*=10.0.

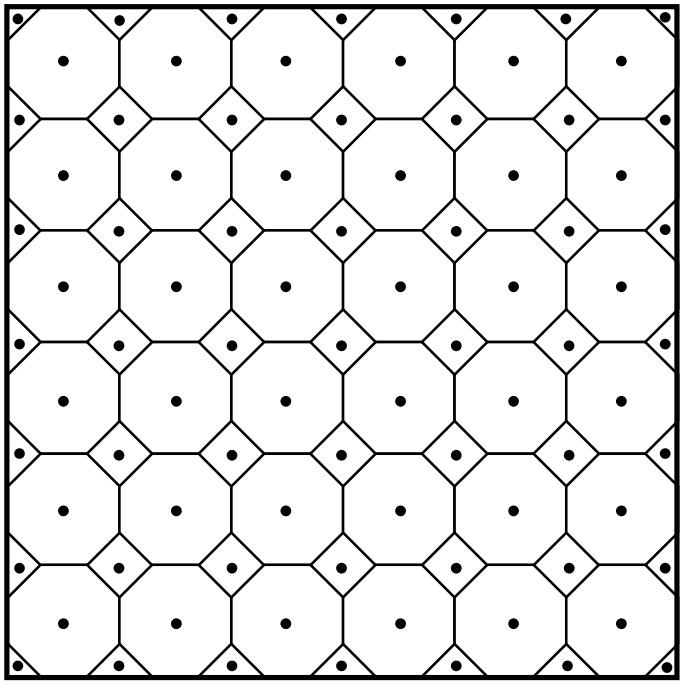

Fig. 2.13 – HGB Grid Model

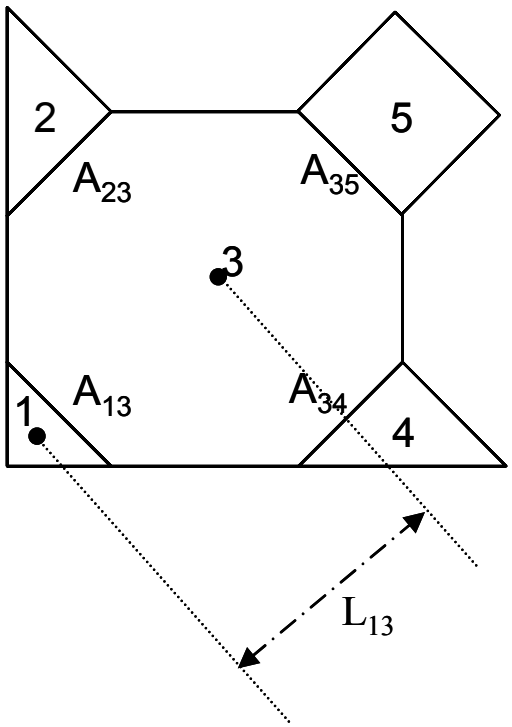

Fig. 2.14 – Example of transmissibilities calculations in HGB

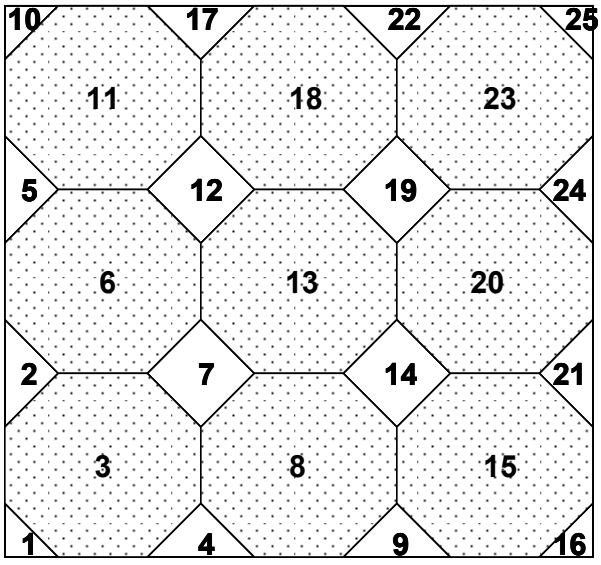

(a)

(b)

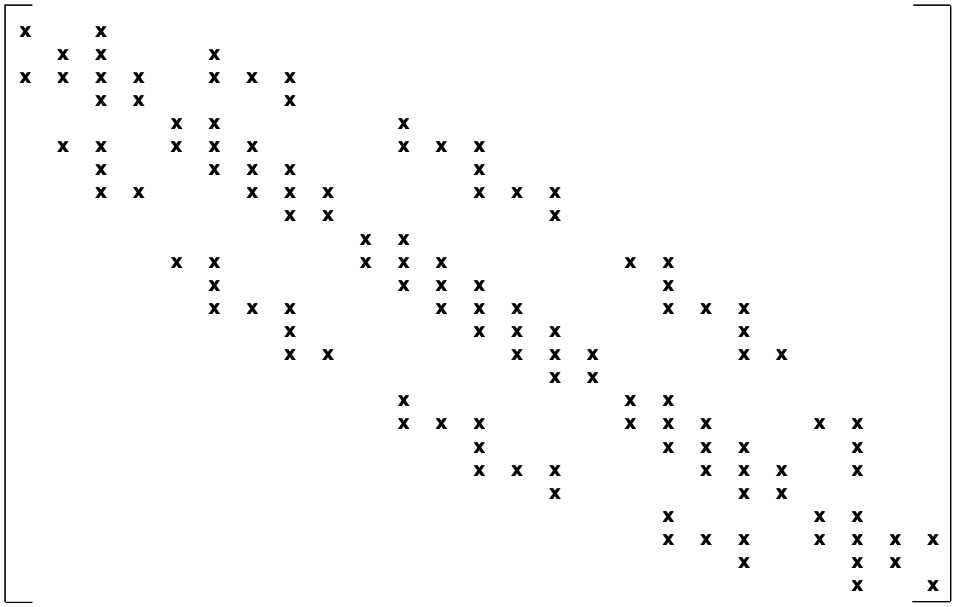

Fig. 2.15 – Diagonal count ordering (a) and the corresponding coefficient matrix (b).

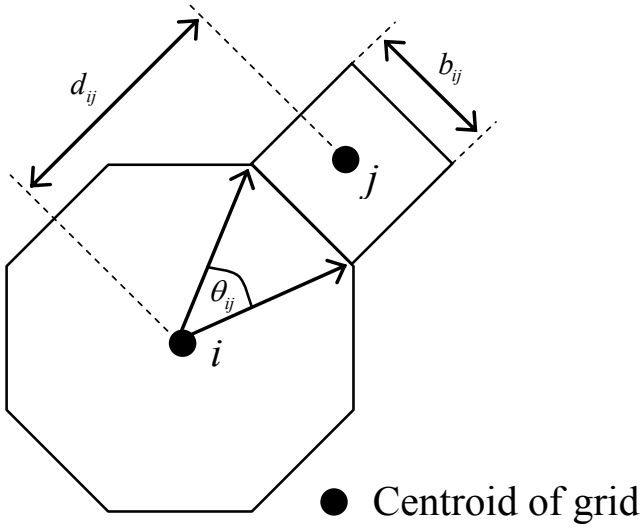

Fig. 2.16 – Well model for a regular polygon

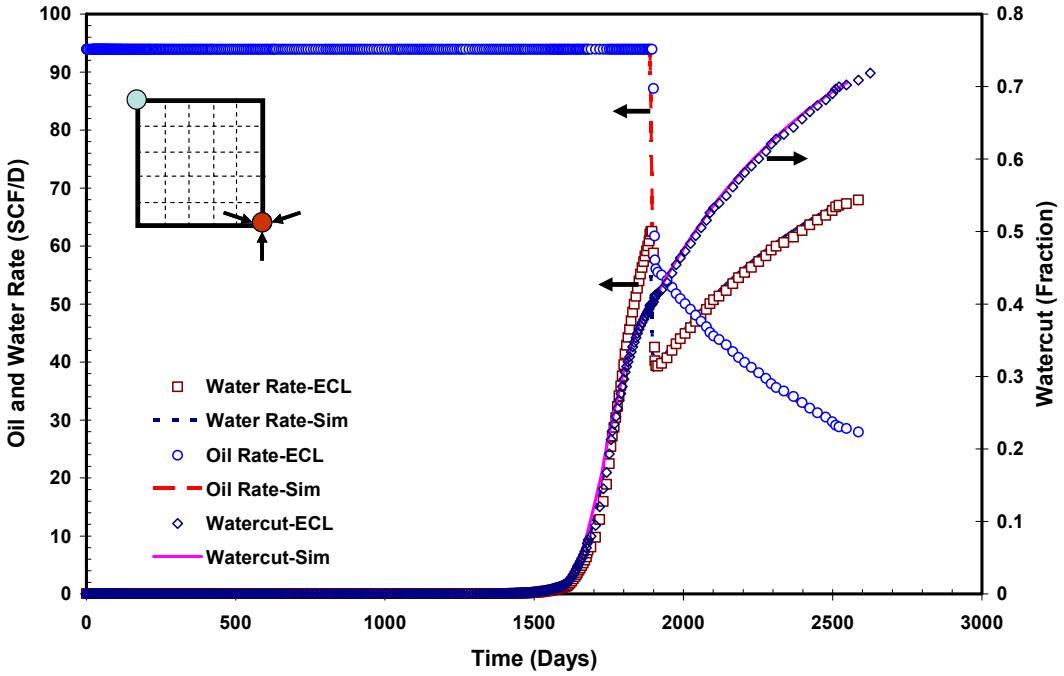

Fig.2.17 – Results of validation between a proposed simulator with an Eclipse 100™.

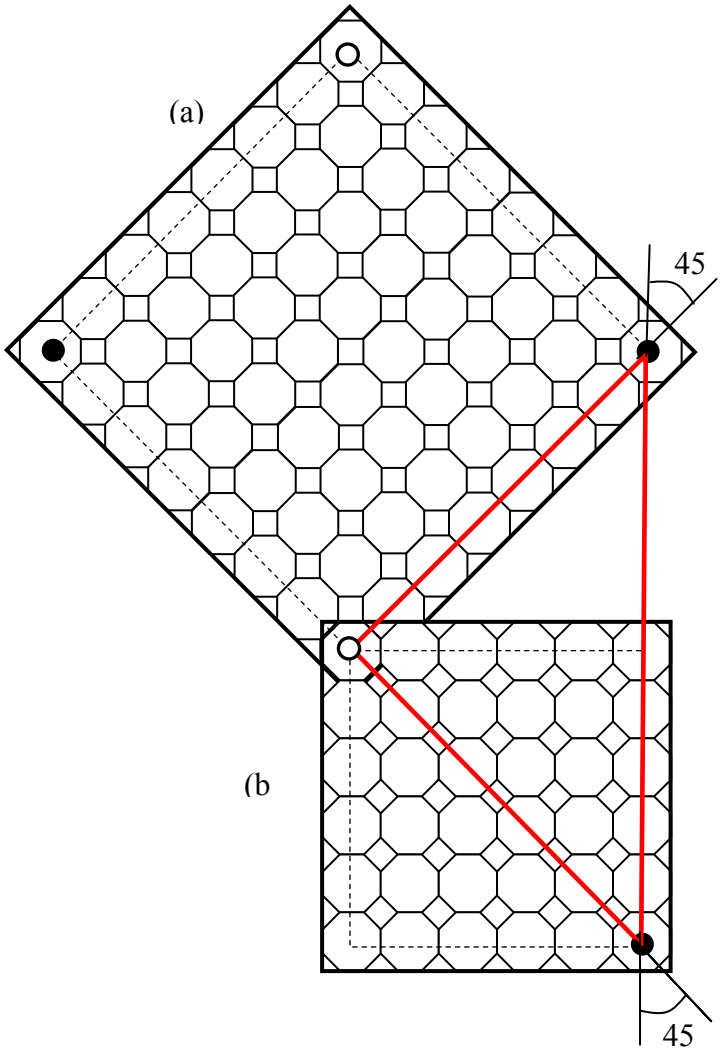

Fig. 2.18 – Example of (a) parallel and (b) diagonal grid orientation in HGB grid

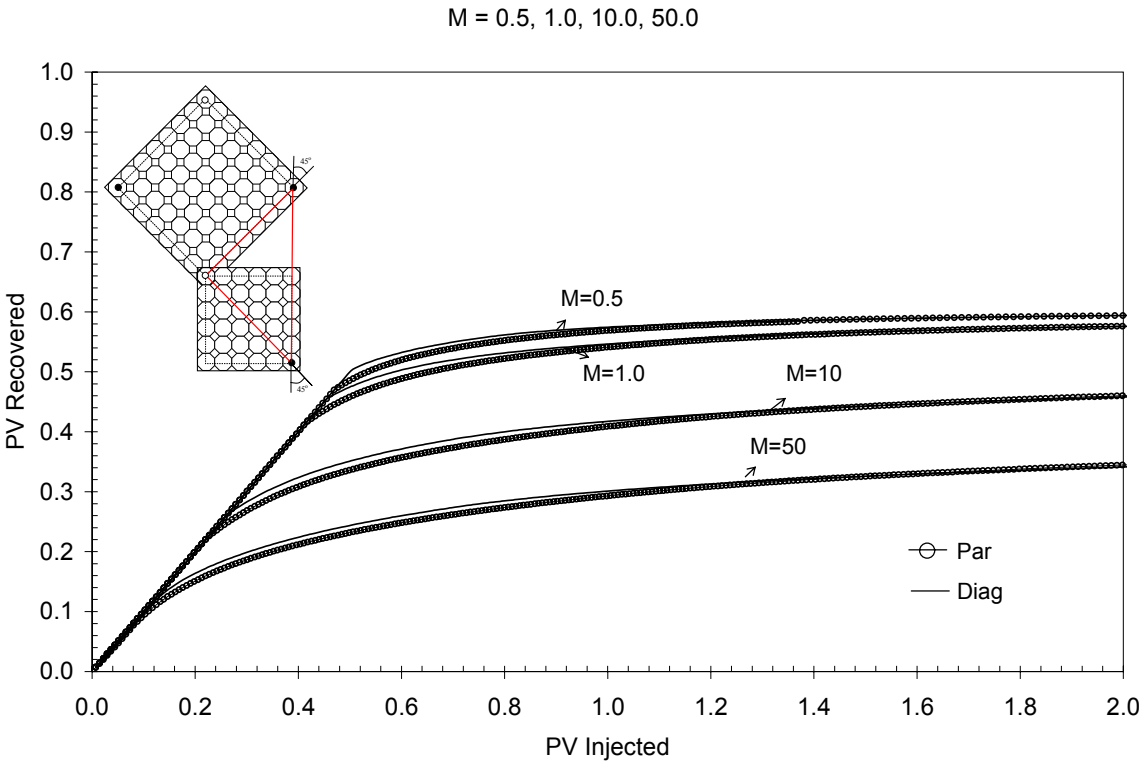

Fig. 2.19 – Influence of mobility ratios on the predicted performance of HGB grid.

M = 0.5	M = 1.0	M = 10	M = 50
	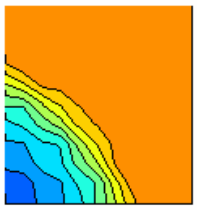	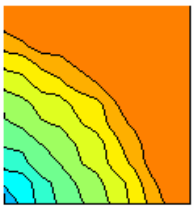	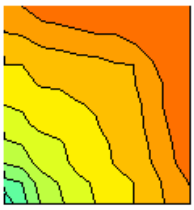
PV_{inj} = 0.1 PV	PV_{inj} = 0.1 PV	PV_{inj} = 0.1 PV	PV_{inj} = 0.1 PV
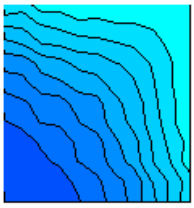	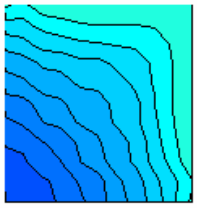	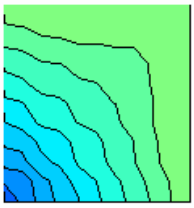	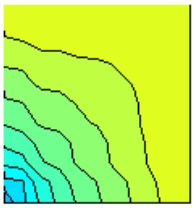
PV_{inj} = 0.5 PV	PV_{inj} = 0.5 PV	PV_{inj} = 0.5 PV	PV_{inj} = 0.5 PV
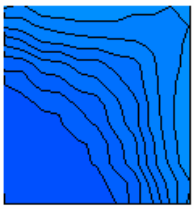	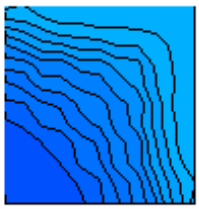	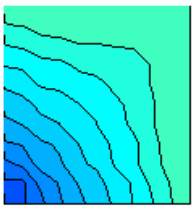	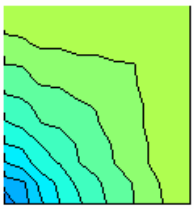
PV_{inj} = 1.0 PV	PV_{inj} = 1.0 PV	PV_{inj} = 1.0 PV	PV_{inj} = 1.0 PV

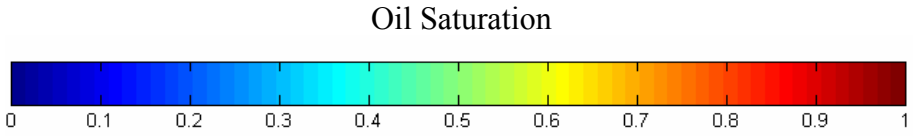

Fig. 2.20 – Saturation distribution map for diagonal HGB grid as shown in Fig. 2.18 (b) at various mobility ratios

M = 0.5	M = 1.0	M = 10	M = 50
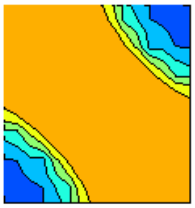	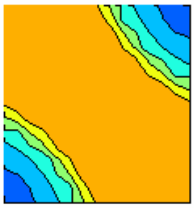	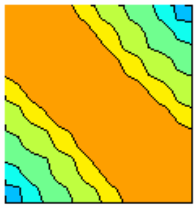	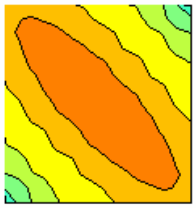
PV_{inj} = 0.1 PV	PV_{inj} = 0.1 PV	PV_{inj} = 0.1 PV	PV_{inj} = 0.1 PV
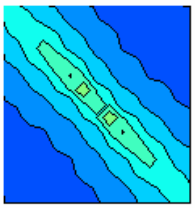	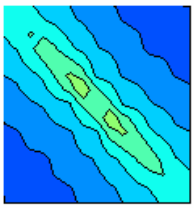	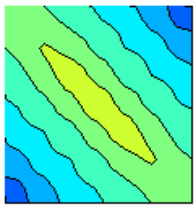	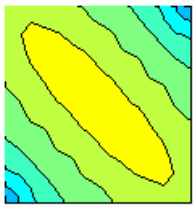
PV_{inj} = 0.5 PV	PV_{inj} = 0.5 PV	PV_{inj} = 0.5 PV	PV_{inj} = 0.5 PV
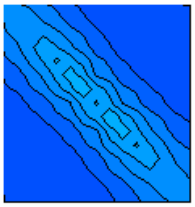	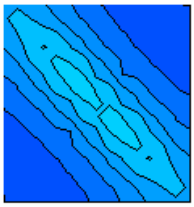	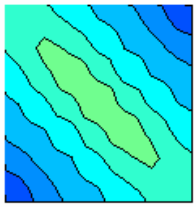	
PV_{inj} = 1.0 PV	PV_{inj} = 1.0 PV	PV_{inj} = 1.0 PV	PV_{inj} = 0.5 PV

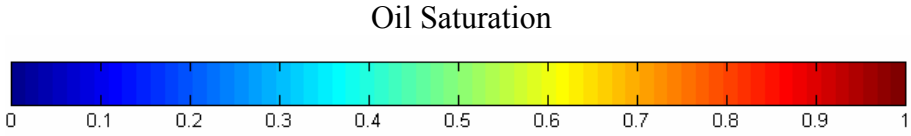

Fig. 2.21 – Saturation distribution map for parallel HGB grid as shown in Fig. 18 (a) at various mobility ratios

APPENDIX A: PROJECT FACT SHEET

CONTRACT TITLE: Investigation of Efficiency Improvement During CO_2 Injection in Hydraulically and Naturally Fractured Reservoirs

ID NUMBER: DE-FC26-01BC15361 **B&R CODE:** AC1005000	**CONTRACTOR:** Texas Engineering Experiment Station **ADDR:** 322 Wisenbaker Engineering Research Center College Station, TX 77843
DOE PROJECT MANAGER: **NAME:** Daniel J. Ferguson **LOCATION:** NPTO **PHONE:** 918/ 699-2047 **E-MAIL:** dan.ferguson@npto.doe.gov	**CONTRACT PROJECT MANAGER:** **NAME:** David Schechter **PHONE:** 979/ 845-2275 **FAX:** 979/845-1307 **E-MAIL:** schech@spindletop.tamu.edu
PROJECT SITE **CITY:** College Station **STATE:** TX **CITY:** **STATE:** **CITY:** **STATE:**	**CONTRACT PERFORMANCE PERIOD:** 9/28/2001 to 9/27/2005 **PROGRAM:** Exploration & Production **RESEARCH AREA:** **PRODUCT LINE:** ADIS

CO-PARTICIPANTS:

PERFORMER:	**CITY:**	**STATE:**	**CD:**
PERFORMER:	**CITY:**	**STATE:**	**CD:**
PERFORMER:	**CITY:**	**STATE:**	**CD:**
PERFORMER:	**CITY:**	**STATE:**	**CD:**

FUNDING (1000'S)	DOE	CONTRACTOR	TOTAL
PRIOR FISCAL YRS	0	0	0
FY 2001 CURRENT OBLIGATIONS	309	78	387
FUTURE FUNDS	628	157	785
TOTAL EST'D FUNDS	937	235	1172

OBJECTIVE: The objective of this project is to perform unique laboratory experiments with Artificial fractured cores (AFCs) and X-ray CT to examine the physical mechanisms of bypassing in HFR and NFR that eventually result in less efficient CO_2 flooding in heterogeneous or fracture-dominated reservoirs. Core flooding experiments in artificially fractured and oil-saturated cores at reservoir conditions will be performed under different conditions of fracture configurations and fracture aperture distributions to investigate matrix-fracture transfer mechanisms. The fluid flow and fracture aperture distributions will be imaged in-situ and real time using X-ray CT. The benefit of WAG in highly heterogeneous reservoirs will be determined. Various CO_2 injection rates, above and below the MMP, will be performed to optimize the operating injection rate and minimize bypassed oil as a result of hydraulic or natural fractures. Numerical analysis will be conducted to model the physical mechanisms of bypassing oil. Results will be important in modeling actual physical mechanisms during CO_2 injection.

PROJECT SUMMARY

Background:

The primary goal of this research is to maximize the potential of CO_2 flooding in the domestic U.S. As more technical knowledge accumulates it becomes clear that natural and hydraulically induced fractures often dominate pattern reservoir or sweep efficiency. As the level of sophistication grows, low permeability reservoirs become more amenable to Enhanced Oil Recovery (EOR) via CO_2. Low permeability reservoirs are usually characterized by brittle matrix rock, which cracks under natural or induced conditions.

Many of the issues involved in saturation distribution during CO_2 injection have been tested in Berea cores above and below miscibility pressure. However, the level of heterogeneity rarely, if ever, includes the presence of natural fractures. This is not coincidental since the level of experimentation required is high in order to develop useful interpretations. The fact remains, however, that reservoir heterogeneity dominates the performance of gas injection. Hydraulic or natural fractures can exert a major influence on the economics of CO_2 injection projects. However, the fundamental mechanisms of transfer in fracture systems are virtually unexplored. The transfer of injected gas from HF or NF determines the ultimate displacement and sweep efficiency. It is the intent of this proposed work to advance the understanding of this dynamic process and determine the implications on the ultimate performance of bypassing reserves during CO_2 injection.

Work to be performed:

Task 1.0 Experimental Investigation of Transfer Mechanisms during CO_2 Flooding in NFR and HFR.

1. Laboratory results to demonstrate the effect of overburden pressure (stress-state) on fracture aperture distribution and permeability of the rock (level of heterogeneity).
2. Effect of fracture aperture distribution on viscous and capillary forces.
3. Laboratory results to demonstrate the effect of hydraulic fracture on sweep efficiency and fracture-matrix interactions.

Task 2.0 Experimental Investigation of Bypassing Mechanisms during CO_2 Flooding in HFR and NFR.

1. Laboratory results showing optimum WAG injection ratio that maximizes the sweep efficiency.
2. Laboratory results showing optimum injection rate that mitigates bypassing oil reserve during CO_2 injection in HFR and NFR.
3. Possible strategies to mitigate bypassing mechanisms that will result in less bypassing and more efficient CO_2 flooding in fracture-dominated reservoirs.

Task 3.0 Imaging Experiments Using X-ray CT.

1. Imaging the saturation profile of non-fractured and fractured cores for investigating bypassing mechanisms and modeling purpose

Task 4.0 Analysis and Modeling Transfer and Bypassing Mechanisms.

1. Development of mathematical model and/or numerical modeling to examine the physical mechanisms of bypassing that occur in hydraulically and naturally fractured reservoirs, both above and below the MMP.
2. Identifying important parameters affecting bypassing mechanisms.
3. Providing more confident scaling of field performance from laboratory experiments.

ACCOMPLISMENTS:

Task 1.0 Literature Review

Task 2.0 Experimental Investigation of Transfer Mechanisms during CO_2 Flooding in NFR and HFR.

1. Laboratory results to demonstrate the effect of overburden pressure (stress-state) on unfractured and fractured cores. Quantification of flow path contributors (matrix or fracture) and determination of fracture aperture (width) and matrix and fracture permeability under variable overburden pressures and injection rates.
2. Laboratory results to demonstrate the effect of overburden pressure (stress-state) on unfractured and fractured cores in multiphase flow. The preliminary results of static imbibition experiments are presented as a precursor to image the saturation profiles of non-fractured and fractured cores using X-Ray CT scanner.

3. Establish the fracture aperture calibration.
4. Laboratory results to demonstrate the effect of overburden pressure (stress-state) on fracture aperture distribution and permeability of the rock (level of heterogeneity).
5. Development dual porosity simulator using empirical transfer function.
6. Laboratory results showing optimum WAG injection ratio that maximizes the sweep efficiency.
7. Laboratory results showing optimum injection rate that mitigates bypassing oil reserve during CO_2 injection in HFR and NFR.
8. Possible strategies to mitigate bypassing mechanisms that will result in less bypassing and more efficient CO_2 flooding in fracture-dominated reservoirs.

Task 3.0 Imaging Experiments Using X-ray CT.

1. Imaging the saturation profile of non-fractured and fractured cores at spontaneous experiments for investigating fluid intake (capillary force) and for modeling spontaneous imbibition.
2. Imaging the movement of brine in oil saturated core.
3. Imaging the movement of brine in a fractured core horizontally and vertically for verifying the use of parallel plate model.
4. Imaging the fractured core for establishing fracture aperture calibration.
5. Imaging the fractured cores for examining fracture aperture distribution under different overburden pressure.
6. Imaging the saturation profile of non-fractured and fractured cores for investigating bypassing mechanisms during CO_2 flooding.
7. Imaging the polymer gels to mitigate bypassing mechanisms that will result in less bypassing and more efficient CO_2 flooding in fracture-dominated reservoirs.

Task 5.0 Analysis and Modeling Transfer and Bypassing Mechanisms.

1. Modeling the laboratory experiment to investigate of the effect of fracture aperture at variable overburden pressures.
2. Modeling fluid flow through a single fracture using experimental, stochastic and simulation approaches to investigate the effect of different rock heterogeneity on flow path contributors.
3. Validation of cubic law equation.
4. Modeling study to investigate the effect of different rock heterogeneity on flow path contributors.
5. Modeling study to investigate the transfer mechanism during core flooding in fractured core.
6. Modeling study to investigate the effect of grid orientation in high mobility ratio

PROJECT STATUS
Current Work:

Task 5.0 Analysis and Modeling Transfer and Bypassing Mechanisms.

1. Modeling CO_2 flooding in non-fractured and fractured cores

SCHEDULED MILESTONES:

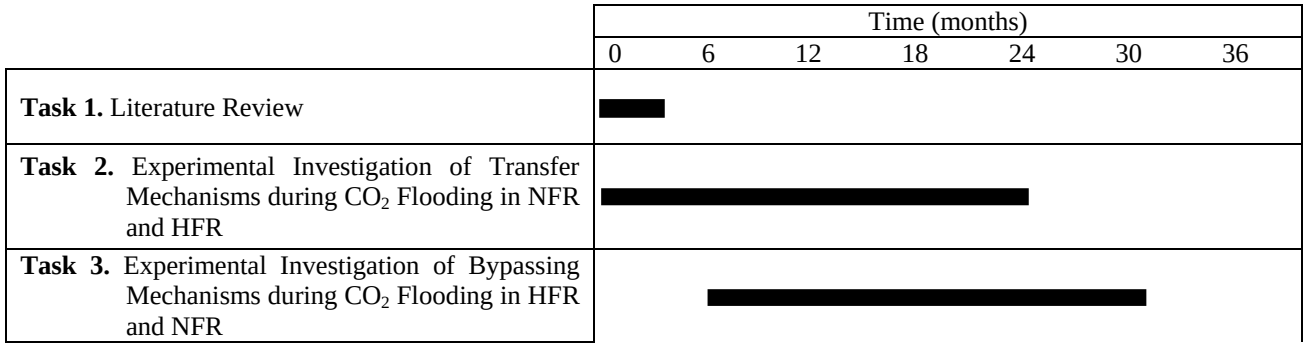

Task 4. Imaging Experiments Using X-ray CT	
Task 5. Analysis and Modeling Transfer and Bypassing Mechanisms	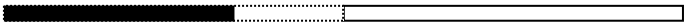
Task 6. Technology Transfer	

Accomplished Milestones
Proposed Milestones

REPORTS:

Putra, E., Schechter, D.S., and Vivek, M.: "Effect of Overburden Pressure on Unfractured and Fractured Permeability Cores," report included in "Investigation of Efficiency Improvement during CO_2 Injection in Hydraulically and Naturally Fractured Reservoirs" First Semi-Annual Progress Report (DOE Contract No.: DE-FC26-01BC15361), Oct 2001-March 2002.

Alfred, D., Muralidharan, V., Putra, E., and Schechter, D.S.: "Modeling Fluid Flow through Single Fracture Using Experimental, Stochastic and Simulation Approaches," report included in "Investigation of Efficiency Improvement During CO_2 Injection in Hydraulically and Naturally Fractured Reservoirs" Second Semi-Annual Progress Report (DOE Contract No.: DE-FC26-01BC15361), April 2002-October 2002.

Muralidharan, V., Putra, E., and Schechter, D.S.: "Investigating the Changes in Matrix and Fracture Properties and Fluid Flow under Different Stress-state Conditions," report included in "Investigation of Efficiency Improvement During CO_2 Injection in Hydraulically and Naturally Fractured Reservoirs" Second Semi-Annual Progress Report (DOE Contract No.: DE-FC26-01BC15361), April 2002-October 2002.

Muralidharan, V., Kaul S., Putra, E., and Schechter, D.S.: "Preliminary Results of Imaging Imbibition Process Using X-Ray CT Scanner," report included in "Investigation of Efficiency Improvement during CO_2 Injection in Hydraulically and Naturally Fractured Reservoirs" Second Semi-Annual Progress Report (DOE Contract No.: DE-FC26-01BC15361), April 2002-October 2002.

Kaul, S., Putra, E., and Schechter, D.S.: "X-Ray Tomography Results Validate Numerical Modeling of Flow in Fractures," report included in "Investigation of Efficiency Improvement during CO_2 Injection in Hydraulically and Naturally Fractured Reservoirs," Third Semi-Annual Progress Report (DOE Contract No.: DE-FC26-01BC15361), October 2002-March 2002.

Tellapaneni, P.K., Putra, E., and Schechter, D.S: "Simulation of Naturally Fractured Reservoirs Using Empirically Derived Transfer Function," report included in "Investigation of Efficiency Improvement during CO_2 Injection in Hydraulically and Naturally Fractured Reservoirs," Fourth Semi-Annual Progress Report (DOE Contract No.: DE-FC26-01BC15361), April 2003-October 2003.

Muralidharan, V., Chakravarthy D., Putra, E., and Schechter, D.S.: "Fracture Aperture and Fracture Distribution," report included in "Investigation of Efficiency Improvement during CO_2 Injection in Hydraulically and Naturally Fractured Reservoirs" Fourth Semi-Annual Progress Report (DOE Contract No.: DE-FC26-01BC15361), April 2003-October 2003.

Chakravarthy D., Muralidharan, V., Putra, E., and Schechter, D.S.: "Application of X-Ray CT for Investigating Effect of CO_2 Injection Rates on Oil Recovery," report included in "Investigation of Efficiency Improvement during CO_2 Injection in Hydraulically and Naturally Fractured Reservoirs" Fifth Semi-Annual Progress Report (DOE Contract No.: DE-FC26-01BC15361), Nov 2003-March 2004.

Chakravarthy D., Muralidharan, V., Putra, E., and Schechter, D.S.: "Possible Strategies to Mitigate CO2 Flooding Bypassing Mechanisms in Fracture-Dominated Reservoirs," report included in "Investigation of Efficiency Improvement during CO_2 Injection in Hydraulically and Naturally Fractured Reservoirs" Fifth Semi-Annual Progress Report (DOE Contract No.: DE-FC26-01BC15361), Nov 2003-March 2004.

Muralidharan, V., Chakravarthy D., Putra, E., and Schechter, D.S.: "Simulation of Fluid Flow through Rough Fractures" report included in "Investigation of Efficiency Improvement during CO_2 Injection in Hydraulically and Naturally Fractured Reservoirs" Sixth Semi-Annual Progress Report (DOE Contract No.: DE-FC26-01BC15361), April 2004-October 2004.

Chong, E., Syihab, Z., Putra, E., and Schechter, D.S.: "A Unique Grid-Block System for Improved Grid Orientation" report included in "Investigation of Efficiency Improvement during CO_2 Injection in Hydraulically and Naturally Fractured Reservoirs" Sixth Semi-Annual Progress Report (DOE Contract No.: DE-FC26-01BC15361), April 2004-October 2004.

TECHNOLOGY TRANSFER ACTIVITIES:

Presentations

On Sept 26, 2004, we (Vivek Muralidharan) presented the talk, "Simulation and Imaging Experiments of Fluid Flow through a Fracture Surface: A New Perspective," for SPE International Student Paper Competition in Houston.

On 9 June, 2004, we (Vivek Muralidharan) presented the talk, "Experimental and Simulation Analysis of Fractured Reservoir Experiencing Different Stress Conditions," for CIPC 2004-229 at 2004 Annual Technical Meeting of the Petroleum Society, Calgary, Canada.

On 9 June, 2004, we (Vivek Muralidharan) presented the talk, "Investigating Fracture Aperture Distributions under Various Stress Conditions Using X-Ray Scanner," for CIPC 2004-230 at 2004 Annual Technical Meeting of the Petroleum Society, Calgary, Canada.

On 10 June, 2004, we (Deepak Chakravarthy) presented the talk, "Application of X-Ray CT for Investigating CO_2 and WAG Injection in Fractured Reservoirs," for CIPC 2004-232 at 2004 Annual Technical Meeting of the Petroleum Society, Calgary, Canada.

On April 17-21, 2004, we presented the talk, "Modeling Fluid Flow through Single Fractures Using Experimental, Stochastic and Simulation Approaches," for SPE/DOE 89442 at 2004 Improved Oil Recovery Symposium, OK.

On March, 2004, we (Vivek Muralidharan) presented the talk, "Simulation and Imaging Experiments of Fluid Flow through a Fracture Surface: A New Perspective," for 2004 Student Research Week Competition in Texas A&M University and won the first place.

On February 16, 2004, we (Vivek Muralidharan) presented the talk, "Simulation and Imaging Experiments of Fluid Flow through a Fracture Surface: A New Perspective," for 2004 SPE Texas A&M contest and won first place in first round and 1st place in final round MS division of Texas A&M. Vivek represented Texas A&M at Regional Region at Texas Tech University, April 2004 and won first place. He will compete in International Region at 2004 SPE Annual Meeting, Houston and at Calgary University, Canada, June 2004.

On February 16, 2004, we (Deepak Chakravarthy) presented the talk, "Application of X-Ray CT to Investigate Effect of Rock Heterogeneity and Injection Rates during CO_2 Flood Process," for 2004 SPE Texas A&M contest and won first place in first round MS division of Texas A&M. Deepak will represent Texas A&M at International Region at Calgary University, Canada, June 2004.

On February 16, 2004, we (Emeline Chong) presented the talk, "Development of a Reservoir Simulator with Unique Grid-Block System," for 2004 SPE Texas A&M contest and won second place in first round MS division of Texas A&M.

On February 16, 2004, we (Orkhan H Pashayev) presented the talk, “Imbibition Assisted Recovery,” for 2004 SPE Texas A&M contest and won third place in first round MS division of Texas A&M.

On February 16, 2004, we (Prasanna K Tellapaneni) presented the talk, “Usage of X-ray CT in Dual Porosity Simulation,” for 2004 SPE Texas A&M contest and won second place in first round PhD division of Texas A&M.

On September 18, 2003, we presented the talk “Waterflood and CO_2 performance in the Naturally Fractured Spraberry Trend Area,” at the Statoil Research Summit 2003, Trondheim, Norway.

On February 8, 2003, we (Dicman Alfred) presented the talk, “Modeling Flow through Fractures using Experimental, Stochastic and Simulation Approaches,” for 2003 SPE Texas A&M contest and won 2nd place in first round and 1st place in final round MS division of Texas A&M. Dicman represented Texas A&M at Regional Region at Rice University and International Region at Calgary University, Canada and won 2^{nd} place at both regions.

On February 8, 2003, we (Sandeep P. Kaul) presented the talk, “X-Ray Tomography Results Validate Numerical Model of Flow in Fractures,” for 2003 SPE Texas A&M contest and won 2nd place in first round MS division of Texas A&M.

On February 8, 2003, we (Vivek Muralidharan) presented the talk, “overburden pressure affects fracture aperture and fracture permeability in a fractured reservoir,” for 2003 SPE Texas A&M contest and won 2nd place in first round MS division of Texas A&M.

On June 2003, we presented the Short Course for Saudi Aramco in Al Khobar, Saudi Arabia – “Reservoir Characterization, Engineering and Enhanced Oil Recovery in Naturally Fractured Reservoirs.”

On March 2003, we presented the Short Course for UNAM/PEMEX in Mexico City, Mexico – “Reservoir Characterization and Engineering in Naturally Fractured Gas and Oil Reservoirs – Part II.”

On June 13, 2002, we presented the "Imbibition and its Relevance to Waterflood Performance in the Naturally Fractured Spraberry Trend Area," at the Rice University and University of Houston invited lecture for Society of Petroleum Engineering Chapter, Duncan Hall, Rice University.

On October 2001, we presented the Short Course for UNAM/PEMEX (National Petroleum Company of Mexico) in Mexico City, Mexico – “Reservoir Characterization and Engineering in Naturally Fractured Gas and Oil Reservoirs - Part I.”

On February 2001, we presented the Short Course for for UNAM/PEMEX in Mexico City, Mexico – “Reservoir Characterization and Engineering in Naturally Fractured Gas and Oil Reservoirs – Part I.”

Papers and Publications

1. Kaul, S.P., Putra, E., and Schechter, D.S.: “Spontaneous Imbibition Simulation with Rayleigh-Ritz Finite Element Method,” paper SPE 90053 will be presented at the 2004 SPE International Petroleum Conference, Puebla, Mexico, 8–9 November.
2. Muralidharan, V., Chakravarthy, D., Putra, E., and Schechter, D.S.: “Simulation of Fluid Flow through Rough Fractures,” paper SPE 89941 will be presented at the 2004 SPE International Petroleum Conference, Puebla, Mexico, 8–9 November.
3. Muralidharan, V., Chakravarthy, D., Putra, E., and Schechter, D.S.: "Simulation and Imaging Experiments for Flow through a Fracture Surface: A New Perspective" paper SPE presented at 2004 International Student Paper Contest, Houston, Texas, 26-29 September.
4. Chong, E., Syihab, Z., Putra, E. and Schechter, D.S.: “A Unique Grid-Block System for Improved Grid Orientation,” paper SPE 88617 will be presented at 2004 Asia Pacific Oil and Gas Conference and Exhibition (APOGCE), Perth, Australia, 18-20 October.

5. Muralidharan, V., Putra, E., and Schechter, D.S.: "Experimental and Simulation Analysis of Fractured Reservoir Experiencing Different Stress Conditions," paper CIPC 2004-229 presented at 2004 Annual Technical Meeting of the Petroleum Society, Calgary, Canada, 8-10 June.
6. Muralidharan, V., Chakravarthy, D., Putra, E., and Schechter, D.S.: "Investigating Fracture Aperature Distributions under Various Stress Conditions Using X-Ray Scanner," paper CIPC 2004-230 presented at 2004 Annual Technical Meeting of the Petroleum Society, Calgary, Canada, 8-10 June.
7. Chakravarthy, D., Muralidharan, V., Putra, E., and Schechter, D.S.: "Application of X-Ray CT for Investigating CO_2 and WAG Injection in Fractured Reservoirs," paper CIPC 2004-232 presented at 2004 Annual Technical Meeting of the Petroleum Society, Calgary, Canada, 8-10 June.
8. Tellapaneni, P.K., Putra, E., and Schechter, D.S.: "Usage of X-Ray CT for Empirical Transfer Functions in Dual Porosity Simulation," paper CIPC 2004-246 presented at 2004 Annual Technical Meeting of the Petroleum Society, Calgary, Canada, 8-10 June.
9. Kaul, S.P., Putra, E., and Schechter, D.S.:"Simulation of Spontaneous Imbibition Using Rayleigh-Ritz Finite Element Method-A Discrete Fracture Approach," paper CIPC 2004-228 presented at 2004 Annual Technical Meeting of the Petroleum Society, Calgary, Canada, 8-10 June.
10. Alfred, D., Putra, E., and Schechter, D.S.: "Modeling Fluid Flow through Single Fractures Using Experimental, Stochastic and Simulation Approaches," paper SPE/DOE 89442 will be presented at 2004 Improved Oil Recovery Symposium, OK, Tulsa, 17–21 April.
11. Alfred, D., Putra, E., and Schechter, D.S., Modeling Fluid Flow Through a Single Fracture Using Experimental, Stochastic and Simulation Approaches, accepted for publication, Saudi Aramco Journal of Technology, Spring, 2004.
12. Putra, E., Muralidharan, V., and Schechter, D.S., Overburden Pressure Affects Fracture Aperture and Fracture Permeability in a Fractured Reservoir, accepted for publication, Saudi Aramco Journal of Technology, Fall 2003.
13. Kaul, S.P., Putra, E., and Schechter, D.S.: "X-Ray Tomography Results Validate Numerical Modeling of Flow in Fractures," Jurnal Teknologi Mineral, 2003

Internet Postings on the Project and Software to Download

A description of our research group can be found at the following Petroleum Engineering Texas A&M Website: http://pumpjack.tamu.edu/faculty/schechter/baervan/homepage.html. The site lists the publications of our group and allows downloads of several papers, reports, and presentations.

This website also allows downloading of software, i.e. spontaneous imbibition simulator, Delaunay Triangulation, reservoir management software (in progress) and reservoir modeling simulator (in progress).

CONTRACT INFORMATION:

NAME: David Schechter
PHONE: 979/ 845-2275
FAX: 979/845-1307
E-MAIL: schech@spindletop.tamu.edu

DIGITAL PICTURES:

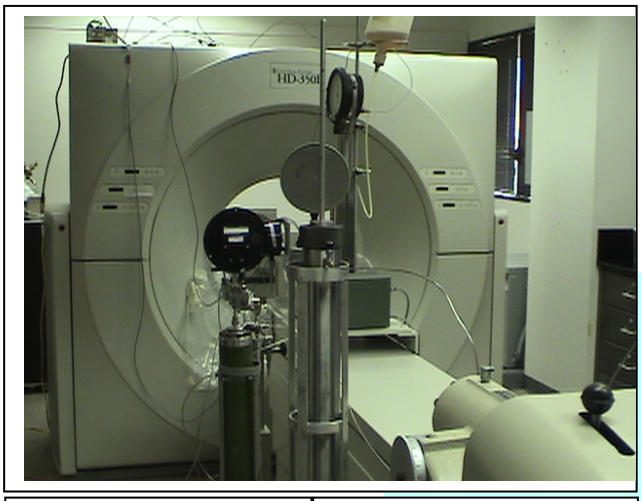

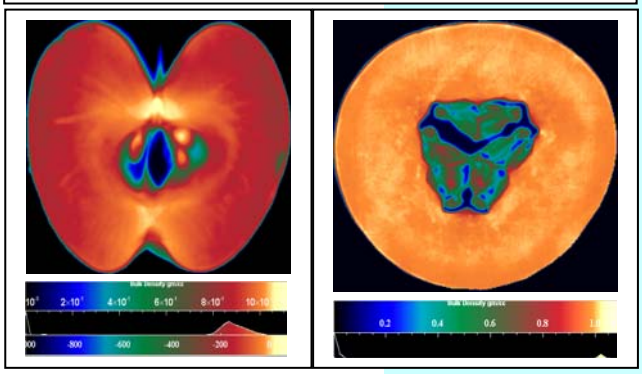

X-Ray CT Scanner Laboratory

The CT Scanner can be used to measure porosity and fluid saturations; to identify phase types and interfaces; and to determine the presence of mineral types and fractures in formation cores. The CT scanner uses the same principle as the basic x-ray. Inside the scanner is a round rotating frame which has x-ray tube mounted on one side and a curved detector on the opposite side. As the frame rotates 360 degrees around the object, a fan of x-rays go through the object to the detector on the opposite side producing a slice image on the digital computer. Measured values are stored as two-dimensional pixel images, which may be combined to create a three-dimensional image of the object scanned.

The CT Scanner uses the combination of the digital computer and rotating x-ray devices to create detailed cross sectional images. The CT Scanner was initially developed and predominantly used as a medical diagnostic tool. With the advent of high-resolution scanners and powerful imaging software has made the CT Scanner increasingly more important as a research and diagnostic tool in petroleum industry.

The HD 350 X-Ray CT Scanner (Fourth Generation) is a state-of-the-art CT scanner capable of scanning objects as large as 50 cm in diameter at scan speeds of 2 seconds per revolution. Acquired in October 2002, the scanner has a cross-sectional resolution of 0.3 mm by 0.3 mm and a fully programmable sample positioning table with a travel precision of 0.03 mm.

To date, the CT Scanner has been used in research projects supported by the U.S Department of Energy for identification fractures and vugs in formation cores, measurement of fracture apertures under different overburden pressure and fluid saturation in fractured cores during waterflood experiments. The CT scanner also is an invaluable research tool for research in other disciplines whenever high-resolution noninvasive diagnostics and measurements are required.